2014

Thermodynamics and crystallography of the γ→ε→α' transformation in FeMnAlSiC steels

Scott Thomas Pisarik

Department:

THERMODYNAMICS AND CRYSTALLOGRAPHY OF THE γ→ε→α' TRANSFORMATION IN FeMnAlSiC STEELS

by

SCOTT THOMAS PISARIK

A THESIS

Presented to the Faculty of the Graduate School of the

MISSOURI UNIVERSITY OF SCIENCE AND TECHNOLOGY

In Partial Fulfillment of the Requirements for the Degree

MASTER OF SCIENCE IN METALLURGICAL ENGINEERING

2014

Approved by

David C. Van Aken, Advisor
Matthew J. O'Keefe
Mohsen Asle Zaeem
Todd M. Link

PUBLICATION THESIS OPTION

This thesis has been prepared in the form of two manuscripts for publication. Pages 17-48 will be submitted for publication in Metallurgical and Materials Transactions A. Pages 49-64 were published 19 April 2014 online and in print in Metallurgical and Materials Transactions A, volume 45A, June 2014. Section 1 (Introduction) and Section 2 (Future Alloy Design) provide supplemental information and discussion to the thesis topic and have been formatted to Missouri University of Science and Technology thesis specification.

ABSTRACT

FeMnAlSiC steels which exhibit two-stage transformation induced plasticity (TRIP) behavior characterized by the γ→ε→α' dual stage martensitic transformation promise to take a leading role in the development of 3rd generation advanced high strength steels. The crystallographic orientation relationship of the γ→α' and γ→ε athermal martensitic transformations in these steels has been determined as the Kurdjumov-Sachs and the Shoji-Nishiyama, respectively. Six crystallographic variants of α-martensite consisting of three twin-related variant pairs were observed in ε- bands. A planar parallelism of {0001}ε || {110}α' and a directional relation of $<1\bar{1}1>\alpha'$ lying within 1° of $<\bar{1}2\bar{1}0>\varepsilon$ existed for these variants. Two regular solution models have been developed to describe the thermodynamics for the γ→ε, γ→α', and subsequent ε→α' martensitic transformations which best described the behavior and microstructure of various FeMnAlSiC TRIP compositions when compared against other thermodynamic models from literature. The role of available nucleating defects of critical size, n^*, has been linked to the intrinsic stacking fault energy (SFE) necessary to observe the athermal γ→ε transformation and it is thus proposed that the amount of ε-martensite in the quenched microstructure is a function of material processing history as well as thermodynamic driving force. The developed thermodynamic model has been used to optimize alloy compositions that produce ideal two-stage TRIP behavior. Compositions with Al contents near 1.5 wt% adequately balance ε- and α-martensite start temperatures such that retained austenite is expected upon quenching to room temperature while also maintaining adequate transformation driving forces to ensure full two-stage TRIP behavior.

ACKNOWLEDGMENTS

This work has been fully supported by the Kent D. Peaslee Steel Manufacturing Research Center as part of the project Development of New 3rd Generation Advanced High Strength Steel. Scanning electron microscopy was performed using an FEI Helios NanoLab dual beam FIB obtained with a Major Research Instrumentation grant from the National Science Foundation under contract DMR-0723128.

I wish to express my extreme gratitude to Dr. David C. Van Aken for his guidance, instruction, and encouragement during my time as both student and researcher. He has passively challenged me every day to push beyond my comfort zone and excel to my maximum potential. I thank him for his everlasting influence on my development as an engineer, scientist, and colleague. I would like to thank Dr. Matthew J. O'Keefe, Dr. Mohsen Asle Zaeem, and Todd M. Link of United States Steel for their role as committee members. Further gratitude is extended to Todd M. Link, Eric Gallo of Nucor Steel, Luis Garza of AK Steel, and Narayan Pottore of AreclorMittal for their advice, support, and technical discussion as acting industry representatives of the Kent D. Peaslee Steel Manufacturing Research Center.

I would like to extend my gratitude to the staff of the Materials Research Center including Dr. Clarissa Wisner and Dr. Jessica TerBush for their guidance and training in electron microscopy and Dr. Eric Bohannon for conducting numerous X-ray Diffraction experiments in support of this project. I also acknowledge my colleagues Daniel Field, Terrell Webb, Kramer Pursell, and Seth Rummel as well as the staff of the Materials Science and Engineering Department for their daily help in overcoming life's daily hurdles. Undergraduate student assistance was provided by Zachary Henderson, Katie Kaczmarek, and Aimee McPherson.

Of special recognition are my loving father and mother, Tom and Ginger Pisarik, and most importantly my fiancée, Jessica Randall, who has been with me in love and support through every step of this most challenging journey. I could not have undertaken such a task without her service as a listener, motivator, helper, confidant, and friend. She joined me in times of doubt and frustration as well as in times of great joy and success.

TABLE OF CONTENTS

LIST OF ILLUSTRATIONS

PAPER II

SECTION

LIST OF TABLES

1. INTRODUCTION

1.1. BACKGROUND

1.1.1. Third Generation Advanced High Strength Steels. For many industries, the increase of efficiency and sustainability while reducing environmental impact is of significant concern. The automotive industry is currently striving to meet a benchmark of 54.5 miles per gallon corporate fuel economy average by 2025 [1]. One avenue of improving fuel efficiency is the light-weighting of the automobile via the reduction of gauge thickness of the metallic components in the body-in-white. To reduce component thickness without sacrificing component strength, and ultimately vehicle and passenger safety, automotive manufacturers are demanding higher strength steels. In an effort to increase energy absorbed upon impact and to maintain ease of manufacturing, these high strength steels must also have significant ductility and formability. Target properties of these new steels have been outlined as combinations of ultimate tensile strengths and elongation to failures of 1000 MPa and 30% or 1500 MPa and 20% [2].

First generation Advanced High Strength Steels (AHSS) including dual phase (DP), TRIP (transformation induced plasticity) and MART (martensitic steels) do not currently meet the target properties as shown in Figure 1.1. While steels belonging to the high-strength, high-ductility second generation AHSS family surpass the property requirements of the automotive sector, they are often expensive to manufacture due to the required large additions of specialty alloying. As such, the development of third generation AHSS which meet the goals of the automotive sector at lower manufacturing cost is paramount.

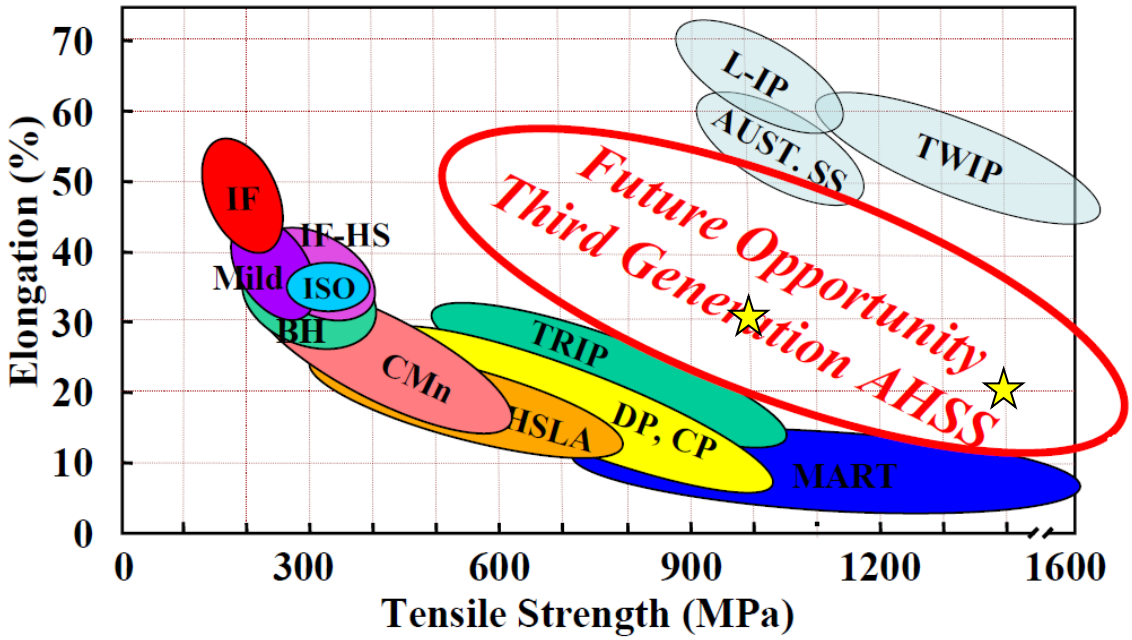

Figure 1.1. Tensile properties of current steel families. Third generation AHSS property goals are 1000 MPa UTS at 30% elongation or 1500 MPa UTS at 20% elongation are denoted by the yellow stars. Figure from [3].

1.1.2. Two-stage Transformation Induced Plasticity. Current first generation Transformation induced plasticity (TRIP) steels typically have a complex microstructure which always contains metastable austenite but may also contain ferrite, martensite, and bainite [4]. Upon plastic deformation, the metastable austenite transforms to α-martensite and delays the onset of necking thereby increasing both ultimate tensile strength and uniform elongation [5]. Steels that exhibit a modified two-stage TRIP behavior where ε-martensite acts as an intermediary phase in a γ→ε→α' transformation have proven to meet and exceed the third generation AHSS benchmarks [6-9]. McGrath et al. [6] have reported exceptional tensile properties of 1165 MPa UTS at 34.4% elongation to failure in a Fe-15.3Mn-2.85Si-2.38Al-0.07C-0.017N steel as shown in Figure 1.2. The steel exhibited a triplex microstructure containing 27% γ-austenite, 60% ε-martensite, and

13% α-martensite that was formed upon water quenching to room temperature after hot rolling and annealing. The predominant strengthening mechanism was attributed to a two-stage TRIP phenomenon characterized by two martensitic transformations: γ→ε and ε→α'. TRIP behavior in the first 5% strain (Stage I) was predominately austenite transforming to ε-martensite as shown in Figure 1.3. Upon saturation of the initial γ→ε transformation, the intermediary ε-martensite transformed to α-martensite (Stage II). A maximum instantaneous work hardening exponent of 1.4 was reported by McGrath et al. [6]. High work hardening rates have been attributed to the TRIP mechanism's segmentation of the austenite into new and smaller phases (ε- and α-martensite), which continuously introduces new dislocation barriers [10-12]. As tensile elongation progresses, the generated strain induced deformation products produce a dynamic Hall-Petch effect by continuously refining grain size and decreasing the dislocation mean free path.

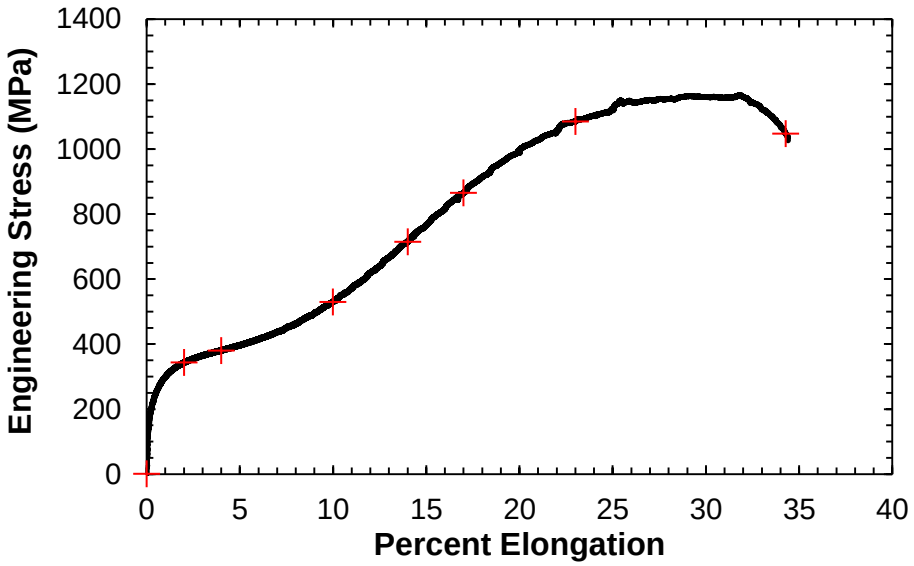

Figure 1.2. Tensile behavior of a Fe-15.3Mn-2.85Si-2.38Al-0.07C-0.017N steel studied by McGrath et al. [6].

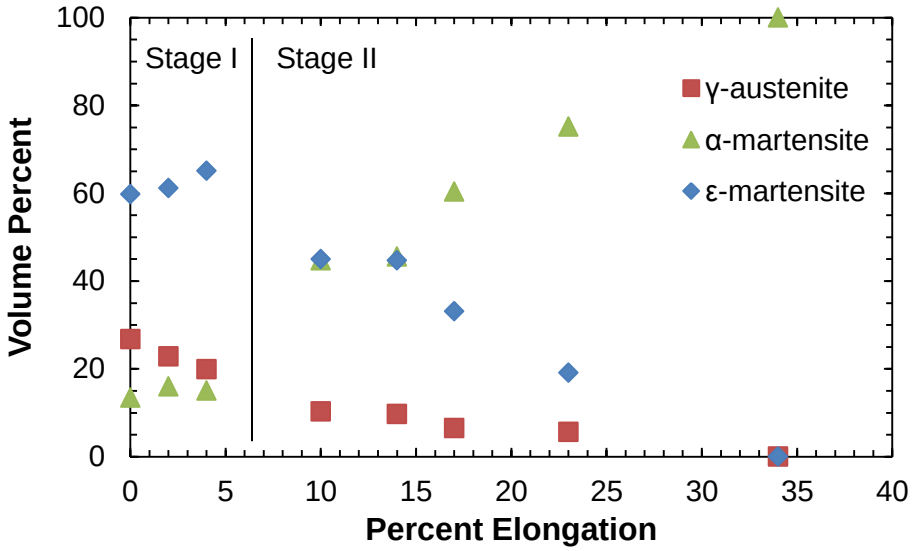

Figure 1.3. Two-stage TRIP behavior in a Fe-15.3Mn-2.85Si-2.38Al-0.07C-0.017N steel studied by McGrath et al. [6].

1.1.3. Stacking Fault Energy. The formation of hexagonal close packed (HCP) ε-martensite can be related to intrinsic stacking fault energy (ISFE) and stacking fault generation. Stacking faults are planar dislocations that alter the stacking sequence of a crystal lattice which induces some change in total energy classified as ISFE [13]. In face-centered cubic (FCC) alloys, a single layer intrinsic stacking fault is associated with a slip <112>{111} expressed in terms of the Burgers vector of the partial dislocation produced during shear, $\mathbf{b}_P$ = 1/6<112>, which changes the stacking sequence of the close packed plane {111} from ABCABCAB to ABCA|CABC where | is the stacking fault [14]. It can be seen that HCP type stacking (i.e. ε-martensite) is developed for the two atomic planes on either side of the stacking fault. In FCC Fe, the required lattice shear for ε-martensite nucleation can be formed by the destabilization of a perfect a/2<110> lattice dislocation into Shockley partial dislocations of the type a/6<112> as depicted in Figure 1.4. Cohen and Olson [15] have shown that the stability of ε-martensite relative to the parent

austenite crystal can be related to the infinite separation of the Shockley partial dislocations when ISFE = 0. The authors expressed the calculation of ISFE as:

$$ISFE = n\rho\left(\Delta G^{\gamma\to\varepsilon} + E^{str}\right) + 2\sigma^{\gamma/\varepsilon} \quad (1.1)$$

where ρ is the planar atomic density of {111}γ (for pure iron: 2.95x10^{-5} mol/m^2), $\Delta G^{\gamma\to\varepsilon}$ is the chemical Gibbs free energy difference between γ-austenite and ε-martensite, E^{str} is the strain energy associated with the transformation, and $\sigma^{\gamma/\varepsilon}$ is the interfacial energy between γ-austenite and ε-martensite which is typically given as 10 ± 5 mJ/m^2 for transition metals [16,17]. The strain energy (E^{str}) is often neglected as it has been shown to contribute less than 0.1% of the measured fault energy [15]. By Eq. (1), the addition of alloying elements that thermodynamically decrease $\Delta G^{\gamma\to\varepsilon}$ (in a negative fashion) when added to the Fe matrix should favor ε-martensite formation.

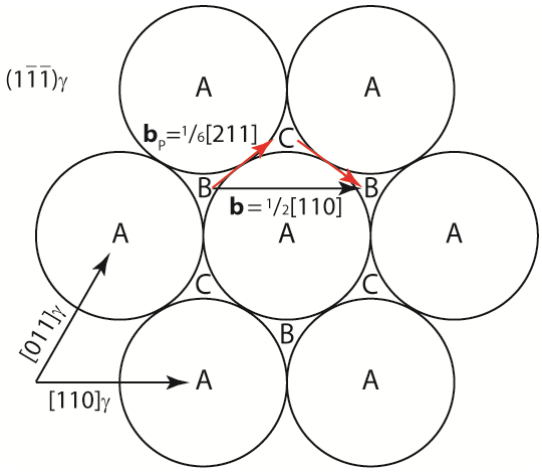

Figure 1.4. The destabilization of a perfect dislocation into two partial dislocations in FCC Fe. A partial dislocation moves a 'B' atom to a 'C' position thereby creating an HCP layer.

Calculation of generalized stacking fault energy (GSFE) as a function of the magnitude of shear <112>{111} has been performed by numerous authors via a first-principles approach [14, 18-20] and produces a GSFE curve similar to that shown in Figure 1.5. In this manner, ISFE can be calculated for a shear displacement of a full $\mathbf{b_p}$ and can be used to describe the stability of ε-martensite relative to the parent austenite. Additionally, it can be seen that a shear displacement of $\frac{1}{2}\mathbf{b_p}$ produces a local maxima in the energy curve called the unstable stacking fault energy (USFE) and is often associated with the energy required to nucleate the Shockley partial dislocation. As such, the value of USFE can be related to the ease of ε-martensite nucleation by its similarity to an activation energy. The effects of manganese and aluminum on the GSFE as calculated via a first principles approach by Medvedeva et al. [18] are shown in Figure 1.6. The parabolic dependence of ISFE on Mn concentration produces the largest stability of ε-martensite at 12-13 at% Mn. In a complex manner, aluminum additions decrease the USFE, potentially making it easier to nucleate ε-martensite, while also increasing the ISFE, resulting in a less stable ε-martensite which may more readily transform to α-martensite.

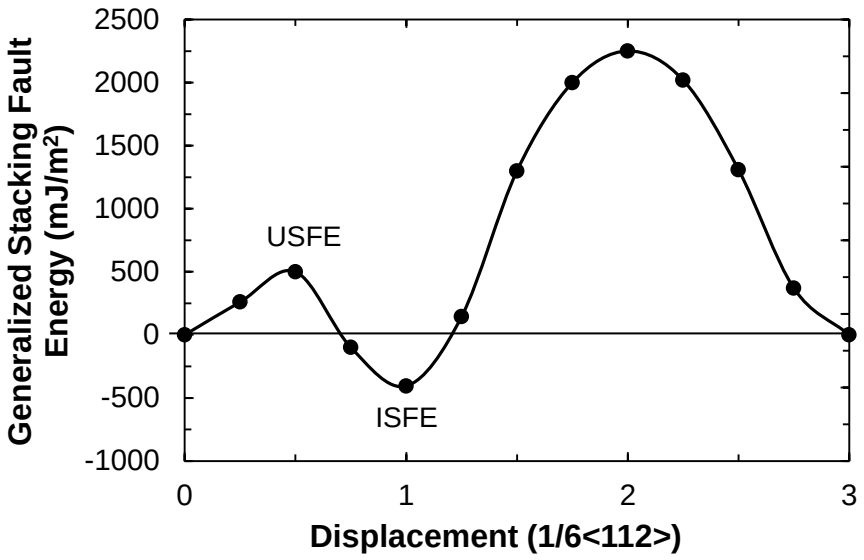

Figure 1.5. Generalized stacking fault energy curve for pure Fe calculated by first-principles simulation. Data taken from Medvedeva et al. [18].

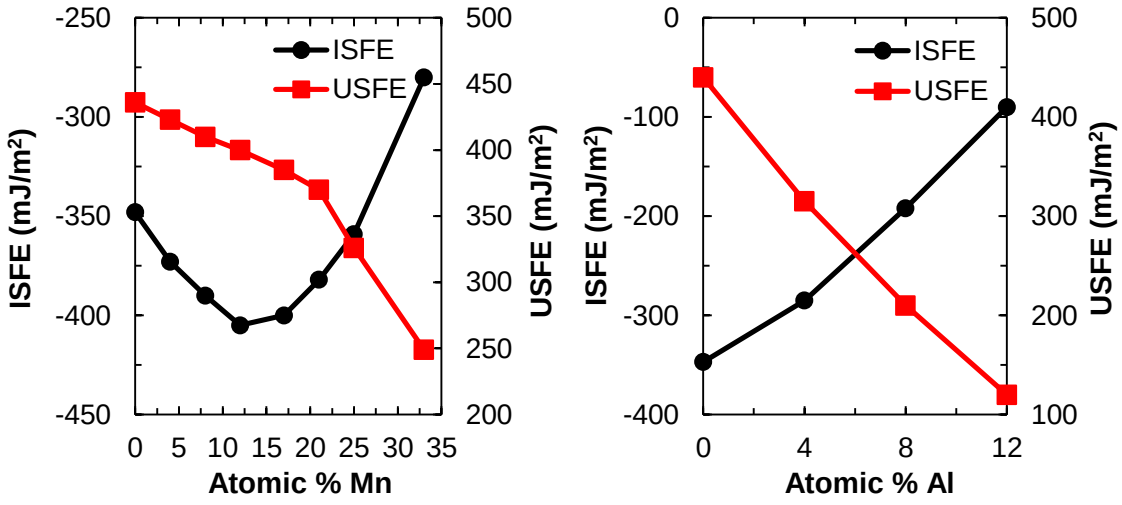

(a) (b)

Figure 1.6. The effect of (a) Mn and (b) Al on the intrinsic and unstable stacking fault energy of FCC Fe. Data taken from Medvedeva et al. [18].

1.1.4. The ε→α' Martensitic Transformation. The athermal and strain induced nucleation of α-martensite in alloys which also exhibit ε-martensite has been observed by numerous authors [21-26]. Of particular interest here is the strain induced ε→α' martensitic transformation associated with Stage II of the two-stage TRIP behavior. The nucleation of α-martensite at the intersection of ε-martensite plates after deformation has been observed by numerous authors in austenitic stainless steels [21-25], FeMnCrNi steels [26] and more recently in the FeMnAlSiC system by McGrath et al. [6]. Strain induced nucleation of α-martensite has also been noted at the intersection of ε-martensite plates with deformation twins [27] and with shear bands of active slip systems [28]. In their seminal work on martensitic transformations, Olson and Cohen [29] described the FCC→BCC transformation in terms of two special twinning shears that provide the necessary invariant plane strains. It can be shown that a one-third twinning shear (T/3) equivalent to $a/18\langle 112\rangle$ on successive $\{111\}_\gamma$ planes in the parent austenite can produce the proper atomic geometry of the $\{110\}_\alpha$ planes of the α-martensite product or embryo. Likewise, a one-half twinning shear (T/2) equivalent to $a/12\langle 112\rangle$ on successive $\{111\}_\gamma$ planes in the parent austenite can produce the proper stacking of the $\{110\}_\alpha$ planes of the α-martensite embryo. It has been proposed that the intersection of the T/3 and T/2 twinning shears is responsible for the strain induced γ→α' transformation as depicted by Figure 1.7 [29]. It can be further shown that the T/2 shear is geometrically equivalent to the distributed shear of the Shockley partial dislocation $a/6\langle 112\rangle$ on every other $\{111\}_\gamma$ which has been previously defined here as an ε-martensite band. The T/3 shear can be expressed in a similar manner as $a/6\langle 112\rangle$ Shockley partial dislocation on every third $\{111\}_\gamma$ plane which could describe a shear band or highly faulted ε-martensite. With this

treatment, the observation of α-martensite nucleation at the intersection of ε-martensite bands with shear bands can be explained. The common nucleation site of dual ε-martensite band intersection can be rationalized by the intersection of one T/2 shear packet with another T/2 shear packet. Here, it is likely that one-third of the partial dislocations of the intersecting T/2 shear packet (ε-martensite band) may be left at the intersection plane, creating a semi-coherent interface, such that now, the effective T/3 shear packet is able to pass through the intersection volume, thereby generating α-martensite. It should be noted that the treatment of Shockley partial dislocations as T/2 and T/3 shear packets requires the "spreading" of the dislocation across the affected two or three atomic planes to form un-faulted BCC stacking as shown in Figure 1.7. While this "spreading" is not likely stable in bulk shear packets such as shear bands or ε-martensite bands, it can be conceptualized as a valid state within the intersection volume during the intersection event. If sufficient stress or chemical driving force is present for transformation, then as the partial dislocations of an intersecting shear packet pass through the intersection volume, the sheared atoms can stick preferentially in BCC lattice positions and be "dragged along" as the other planes are sheared a distance equivalent to the remaining magnitude of the dislocation. This process effectively "spreads" the Shockley partial dislocations [29]. In this manner, the formation of BCC martensite allows the otherwise blocked dislocations of a shear band or ε-martensite plate to pass through the intersected volume and allows continued deformation. FeMnAlSiC [30] and FeMnSiC [31] steels which did not undergo full ε→α' transformation due to the over-stabilization of ε-martensite have exhibited premature tensile fracture and limited ductility. This phenomenon has been related to crack nucleation at the intersection of ε-

martensite plates with each other [32] and with twin boundaries in the parent austenite [33] and are in agreement with the sessile dislocation barrier created by the intersection of two shear packets when sufficient ε→α' transformation driving forces are not present as proposed by Olson and Cohen [29].

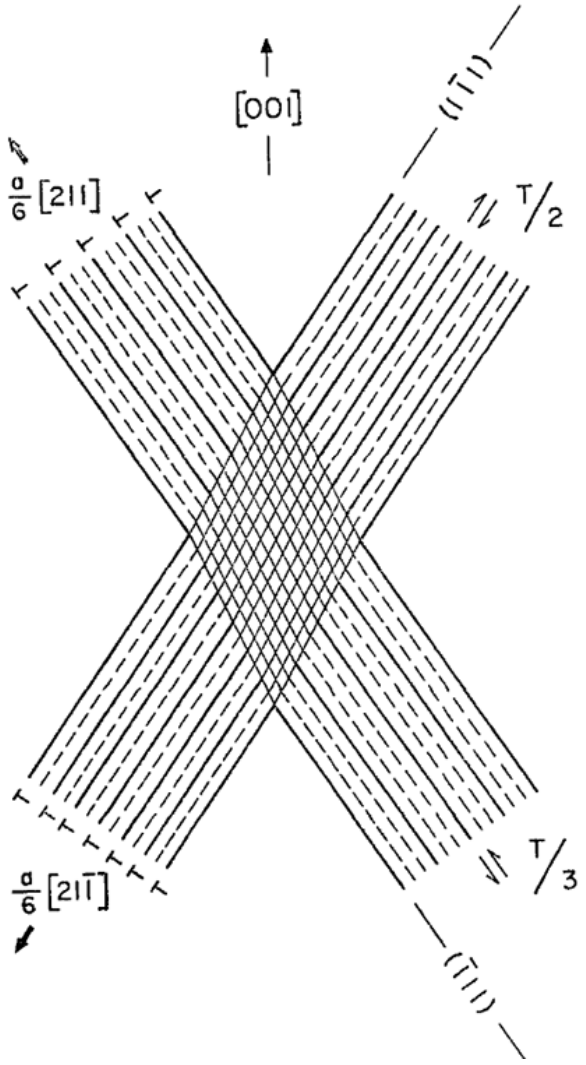

Figure 1.7. The nucleation of α-martensite from the intersection of a T/2 and T/3 shear packet [29].

1.1.5. Current Alloy Design. In order to achieve two-stage TRIP behavior upon deformation, alloying must be strictly controlled to provide favorable ISFE and chemical driving forces for the two stage transformation. The strain induced γ→ε→α' martensitic transformations have been observed in variants of 18Cr-8Ni austenitic stainless steels during deformation at cryogenic [34-36] or room [22-24] temperatures. However, in an effort to reduce alloying costs associated with stainless steel compositions, austenitic steels stabilized by nominal compositions of 15 wt% Mn have garnered increased attention. A survey of Mn bearing alloys from literature which have exhibited the strain induced γ→ε→α' martensitic transformation is listed in Table 1.1. Alloys that contain approximately 15 wt% Mn in conjunction with Si and Al contents between 1-3 wt% and low C contents (< 0.20 wt%) have shown ideal TRIP behavior.

Table 1.1. Alloy compositions in weight pct of Mn bearing steels that exhibited strain induced γ→ε→α' martensitic transformation.

Alloy	C	Mn	Si	Al	N
(A) McGrath et al.[6]	0.07	15.3	2.85	2.4	0.017
(B) Van Aken et al.[7]	0.06	14.2	1.85	2.38	0.019
(C) Pisarik et al.[30]	0.08	15.1	1.95	1.4	0.017
(D) Pisarik et al.[30]	0.16	14.3	2.97	0.89	0.022
(E) Frommeyer et al.[37]	0.02	15.8	3.00	2.9	---
(F) Holden et al.[38]	0.006	15.6	0.13	---	0.009
(G) Grassel et al.[39]	0.02	17.9	1.90	3.5	---

Holden et al. [38] has shown that in the binary Fe-Mn system, there exists several austenite decomposition behaviors controlled by Mn concentration as depicted in Figure 1.8. Compositions near 15 wt% Mn adequately eradicate massive ferrite and bainite

formation while suppressing α-martensite formation in favor of ε-martensite. Holden et al. [38] found that binary alloys between 10-15 wt% Mn gave mixed α'+ε microstructures while alloys between 15-20 wt% Mn produced mixed γ+ε microstructures. The binary Alloy F in Table 1.1 examined by Holden et al. [38] exhibited a room temperature microstructure of 70% ε-martensite and 30% retained austenite and did not form α-martensite until 6% cold reduction was applied. The remaining alloys in Table 1.1, with some combination of Al, Si, and C addition, all exhibited γ+ε+α' triplex microstructures prior to tensile testing.

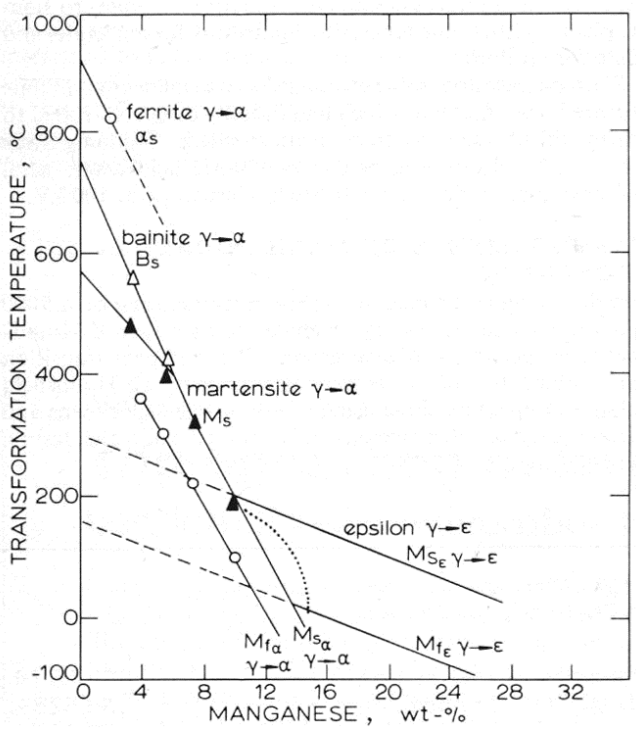

Figure 1.8. The effect of Mn concentration on austenite decomposition mode in binary Fe-Mn alloys [38].

The effect of C content on M_S^{ε} temperature in ternary Fe-17Mn-C steels has been examined by Koyama et al. [12] and is shown in Figure 1.9. Carbon additions greater than 0.2 wt% have been shown to suppress ε-martensite formation to temperatures less than room temperature. As such, the alloys listed in Table 1.1 have C contents near 0.1 wt% to ensure ε-martensite can form both athermally and via the TRIP phenomenon when deformed at room temperature. The $M_S^{\alpha'}$ temperature is also affected by C concentration as indicated by the empirical equation derived by DeCooman and Speer [40] for FeMnAlSiC steels:

$$M_s\left(^{\circ}C\right) = 539 - 423\left[wt\%C\right] - 30.4\left[wt\%Mn\right] - 7.50\left[wt\%Si\right] + 30.0\left[wt\%Al\right] \quad (1.2)$$

Increasing C decreases $M_S^{\alpha'}$ temperature more rapidly (423°C/wt%) than the M_S^{ε} temperature decreases (389°C/wt%). As such, C content can be varied in an attempt to control the relative amounts of athermal ε- and α-martensite in a quenched microstructure.

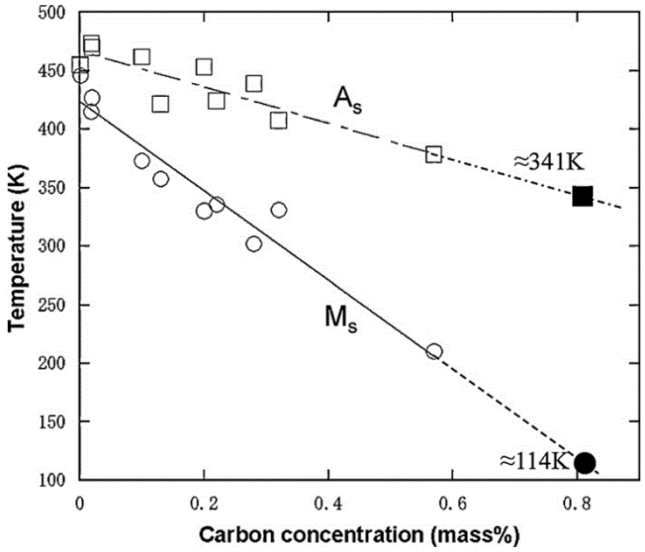

Figure 1.9. The effect of C on ε-martensite start temperature in a Fe-17Mn-C alloy [12].

As has been previously shown by Medvedeva et al. [18], the addition of Al decreases the USFE thereby making the nucleation of Shockley partial dislocations, and ultimately ε-martensite, easier. It has recently been shown by Pisarik et al. [30] via first principles calculation that Si and Al have a similar effect in decreasing USFE while increasing ISFE as shown in Figure 1.10. These calculations are corroborated by the successful nucleation of strain induced ε-martensite in an alloy with increased Si content (2.97 wt%) in substitution for Al (present at 0.89 wt%) [30]. Analyzing the FeMnAlSiC compositions of Table 1.1, in which all alloys exhibited the γ→ε martensitic transformation upon deformation, reveals the combination of Si and Al contents near 3 or 4 wt% is adequate to ensure Shockley partial dislocation nucleation without deleterious effects on ISFE. The substitution of Si for Al is also beneficial in the suppression of δ-ferrite formation as discussed by Pisarik et al. [30].

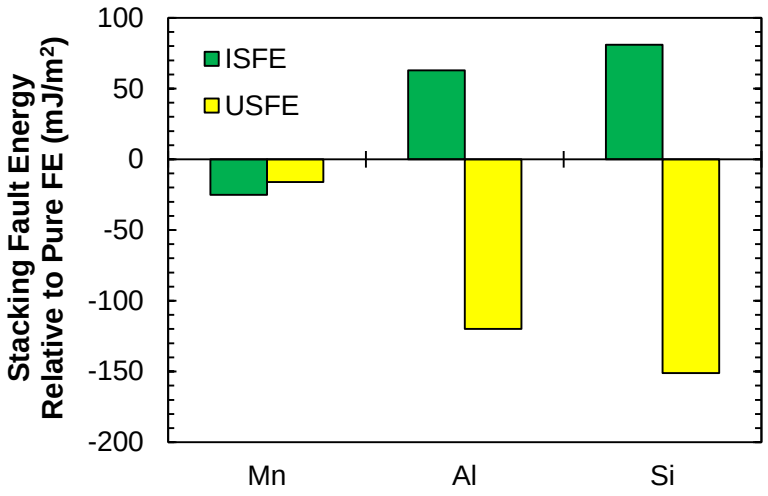

Figure 1.10. The effect of solute elements positioned at a stacking fault on intrinsic and unstable stacking fault energy relative to pure iron as determined by first principles calculations [30].

1.2. PURPOSE AND OBJECTIVE

The continued development of FeMnAlSiC steels which exhibit a two-stage TRIP behavior upon deformation is of pertinent interest in an attempt to achieve the desired strength and ductility benchmarks established by the automotive sector for third generation AHSS. It has been shown that phase stability and strain induced transformations can be influenced by changes in composition, or perhaps more appropriately, changes in chemical driving force. The thermodynamic over-stabilization of ε-martensite has led to early tensile fracture in some steels [30,31] while complete two-stage transformation can result in tensile properties in excess of 1100 MPa UTS and 30% elongation to failure [6,7]. It is therefore prudent to be able to calculate chemical driving forces $\Delta G^{\gamma\rightarrow\varepsilon}$, $\Delta G^{\gamma\rightarrow\alpha'}$, and subsequently $\Delta G^{\varepsilon\rightarrow\alpha'}$ for a given TRIP alloy as these values can give an indication to the nature of the progression of the γ→ε→α' transformation. It is the aim of the work in this thesis to develop a comprehensive, and self-consistent, thermodynamic model that can accurately calculate the transformation driving forces for the FeMnAlSiC alloy system. This work will aid the design of future alloys by providing a predictive tool with which the influence of various alloy additions on the martensitic transformations can be quickly and accurately evaluated.

Of additional interest is the crystallography and orientation preference of the γ→ε→α' martensitic transformation, which to the author's knowledge has not been confirmed for the FeMnAlSiC system. It is the aim of the work in this thesis to utilize orientation image mapping via electron backscattered diffraction analysis to verify the presence of HCP ε-martensite in a FeMnAlSiC steel and to determine nucleation and growth textures associated with the ε→α' transformation. This work will serve to

provide a better understanding of the two-stage martensitic transformation and give some insight into the source of the rapid work hardening exhibited in two-stage TRIP alloys.

PAPER

I. THERMODYNAMIC DRIVING FORCE OF THE γ→ε→α' TRANSFORMATION IN FeMnAlSiC STEELS

S.T. Pisarik and D.C. Van Aken

Department of Materials Science and Engineering

Missouri University of Science and Technology

223 McNutt Hall, 1400 N. Bishop, Rolla, MO 65409-0330, USA

Tel.: 573-341-4717

Email: dcva@mst.edu

To be submitted for publication in Metallurgical and Materials Transactions A

ABSTRACT

Two-stage transformation induced plasticity (TRIP) behavior characterized by the martensitic transformation, $\gamma \rightarrow \varepsilon \rightarrow \alpha'$, has produced exceptional tensile strengths and work hardening rates in FeMnAlSiC alloys. Incomplete transformation via the two-stage process has led to early fracture in some steels where the intermediary ε-martensite was over-stabilized with respect to α-martensite. It is therefore prudent to be able to calculate thermodynamic driving forces for the martensitic transformations to predict TRIP behavior. Utilization of the Thermocalc software package overestimated the $\gamma \rightarrow \varepsilon$ driving force while a regular solution model developed here provides excellent agreement between calculated stacking fault energy and the measured retained austenite fraction. The FactSage software package, the Zener enthalpy model, the Aaronson, Domain and Pound model, and the Bhadeshia model have been eliminated as viable models for the calculation of $\gamma \rightarrow \alpha'$ transformation driving force for this alloy class due to the high solute fraction lying outside the limits of accuracy for each model. A regular solution model has calculated reasonable values of $\Delta G^{\gamma \rightarrow \alpha'}$ which have been used to further calculate $\Delta G^{\varepsilon \rightarrow \alpha'}$. The predicted driving forces for transformation correspond well with the microstructure and behavior of the seven FeMnAlSiC steels from literature compared here when considered in conjunction with strain and interface nucleation energy, nucleating defect critical size, and material process history. The developed regular solution models can therefore be used as a thermodynamic tool in the prediction of the $\gamma \rightarrow \varepsilon \rightarrow \alpha'$ martensitic transformation and the resulting microstructural constituents, and may give some indication to the nature of two-stage TRIP behavior upon deformation if the extent of solute segregation is well understood.

1. INTRODUCTION

The use of transformation induced plasticity (TRIP) steels in new vehicles is expected to increase in an effort to meet the proposed fuel economy standard of 54.5 miles per gallon by 2025 [1]. Projected properties of newly developed TRIP steels range from ultimate tensile strengths (UTS) of 1000-1500 MPa and elongation to failures of 30%-20% [2]. TRIP steels obtain such exceptional properties through strain induced martensitic transformations that subsequently yield high work hardening rates and large ductilities [3]. While most ferrous alloys exhibit stable microstructures during deformation, high manganese TRIP steels possess a metastable microstructure of retained austenite, γ (FCC), which transforms to ε-martensite (HCP), and potentially to α-martensite (BCC), under mechanical load. Two stage TRIP behavior, in which ε-martensite acts as an intermediate phase during the γ→ε→α' transformation, has been observed in multiple studies [2-6]. The stability of either martensite phase during deformation is dependent on the thermodynamic driving forces for transformation of austenite to ε-martensite, $\Delta G^{\gamma\rightarrow\varepsilon}$, and α-martensite, $\Delta G^{\gamma\rightarrow\alpha'}$. Promotion of the ε- to α-martensite transformation through alloy design is of crucial importance in achieving exceptional properties since steels that become saturated with over-stabilized ε-martensite have exhibited premature fracture [6,7]. This phenomenon has been related to crack nucleation at the intersection of ε-martensite plates with each other [8] and with twin boundaries in the parent austenite [9]. Recent FeMnAlSiC steels which exhibited full transformation to α-martensite via the two-stage γ→ε→α' TRIP reaction have achieved superior properties of 1165-1217 MPa ultimate tensile strength at 28.5-34.4% elongation to failure [2,4]. It is therefore prudent to be able to calculate $\Delta G^{\gamma\rightarrow\varepsilon}$, $\Delta G^{\gamma\rightarrow\alpha}$, and

subsequently $\Delta G^{\varepsilon\rightarrow\alpha}$ for a given TRIP alloy as these values can give an indication to the nature of the progression of the γ→ε→α' transformation.

2. STACKING FAULT ENERGY AND ε-MARTENSITE FORMATION

In FCC alloys, a single layer intrinsic stacking fault is associated with the change in stacking sequence of the close packed plane {111} from ABCABCAB to ABCA|CABC where "|" is the stacking fault. Such a fault can be formed in FCC Fe by a slip <112>{111} which can be expressed in terms of the Burgers vector of the partial dislocation produced during shear, $\mathbf{b}_P$ = 1/6<112> [10]. In this manner, the passing of partial dislocations on every other close packed plane produces a bulk hexagonal close packed (HCP) crystal (i.e. ε-martensite). As such, in their pioneering work describing the FCC→HCP transformation, Olson and Cohen [11] have treated the stacking fault as an HCP embryo, two planes in thickness (n=2). Similar to classical nucleation theory, the energy describing the stacking fault can then be described by a volume energy and surface energy component. The stacking fault energy (SFE) for a fault *n* planes in thickness can be calculated by:

$$SFE = n\rho\left(\Delta G^{\gamma\rightarrow\varepsilon} + E^{str}\right) + 2\sigma^{\gamma/\varepsilon} \quad (1)$$

where ρ is the planar atomic density of {111}γ (here: 2.95x10^{-5} mol/m^2), $\Delta G^{\gamma\rightarrow\varepsilon}$ is the chemical Gibbs free energy difference between γ-austenite and ε-martensite, E^{str} is the strain energy associated with the transformation, and $\sigma^{\gamma/\varepsilon}$ is the interfacial energy between γ-austenite and ε-martensite which is typically given as 10 ± 5 mJ/m^2 for transition metals [12,13]. The strain energy (E^{str}) is often neglected as it has been shown to contribute less than 0.1% of the measured fault energy [11].

In FCC metals, it is well known that SFE can be related to the destabilization of perfect a/2<110> lattice dislocations into Shockley partial dislocations of the type a/6<112> responsible for the creation of stacking faults. As shown by Cohen and Olson [11], there exists a dislocation energy governed by the separation distance of the two opposing partials. The restraining force necessary for producing a stable partial separation is provided by positive fault energy. As the volume energy component of Eq. (1) becomes negative, usually via the lowering of temperature, and approaches and surpasses the magnitude of the (positive) surface energy component the SFE will value pass through 0. At this temperature, the uninhibited partial dislocations can separate indefinitely thereby creating an ε-martensite band [11,14]. If thicker faults are considered (i.e. n>2), the volume energy component has a greater effect in lowering the SFE energy to zero such that ε-martensite can form at a higher temperature than as suggested by an intrinsic stacking fault. As such, even though the calculated or measured SFE (n=2) may be positive, the energy of thicker, stacked faults (n>2) can be zero or negative. This phenomenon is depicted schematically in Figure 1. Thicker faults can result from the stacking of lattice dislocations on every other close packed plane. There will be a distribution of n thick nucleating defects in a given material depending on its process history; however the M_S^{ε} temperature can be determined as the temperature at which SFE(n) = 0 for the value of n which nucleates a detectable amount of ε-martensite. The role of thicker faults exhibiting decreased SFE has been observed by Fujita and Ueda [15] during in-situ straining of 18Cr-8Ni stainless steel using transmission electron microscopy. The nucleation of a wide stacking fault induced additional fault formation on adjacent slip planes. This effective thickening of the stacking fault was attributed to a

decrease in nucleating embryo energy. Figure 1 also depicts the inability to form ε-martensite, regardless of nucleating defect size, if the temperature is above T_0 i.e. the temperature at which $\Delta G^{\gamma\rightarrow\varepsilon} = 0$. In this regard, the γ→ε transformation behaves similarly to the T_0 behavior originally proposed by Kaufman and Cohen [16] for the γ→α' transformation in which some degree of undercooling is necessary to nucleate the martensitic phase. The value of SFE at T_0 is therefore $2\sigma^{\gamma/\varepsilon}$ and is related to the commonly reported [3,14,17] metric that the γ→ε transformation via TRIP phenomenon is possible for those alloys with SFE less than 18-20 mJ/m^2.

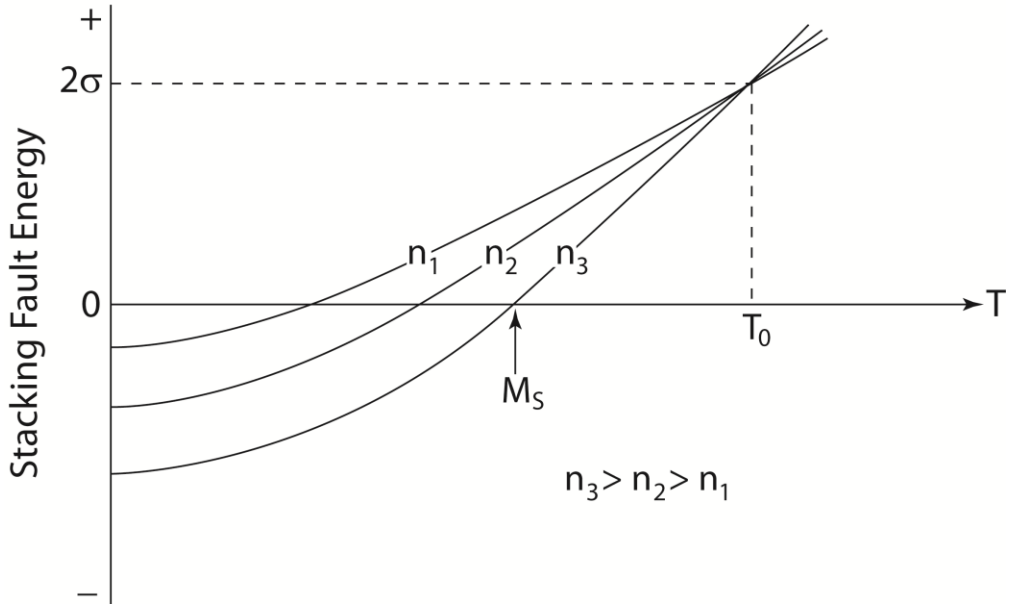

Figure 1. Schematic depiction of the effect of fault thickness on stacking fault energy. The martensite start temperature is associated with the thickest nucleating defect size. Redrawn from Ref [11].

3. A REGULAR SOLUTION MODEL OF THE γ→ε MARTENSITIC TRANSFORMATION

It has been shown that the calculation of SFE is reliant on the Gibbs free energy for the γ→ε phase transformation, $\Delta G^{\gamma\rightarrow\varepsilon}$, which contributes the temperature dependence shown in Figure 1. The change in Gibbs free energy for the transformation can be expressed using a regular solution model as based on the original work of Breedis and Kaufman [18] and has been applied by numerous authors in Fe-Mn [19], Fe-Mn-C [20], Fe-Mn-Al-C [12] alloy systems according to the expression:

$$\Delta G^{\gamma\rightarrow\varepsilon} = X_{Fe}\Delta G_{Fe}^{\gamma\rightarrow\varepsilon} + \sum X_i \Delta G_i^{\gamma\rightarrow\varepsilon} + \sum X_{Fe} X_i \Delta\Omega_{Fe(i)}^{\gamma\rightarrow\varepsilon} \quad (2)$$

where X_i is the atomic fraction of any solute element, *i*, and the summation accounts for all alloying elements which in this study include C, Mn, Si, and Al. The values of the Gibbs free energy change for an alloying element's γ→ε transformation, $\Delta G_i^{\gamma\rightarrow\varepsilon}$, and its interaction energy parameter with an iron based solid solution, $\Delta\Omega_{Fe(i)}^{\gamma\rightarrow\varepsilon}$, can be calculated using:

$$\Delta G_i^{\gamma\rightarrow\varepsilon} = G_i^{\circ\varepsilon} - G_i^{\circ\gamma} \quad (3)$$

$$\Delta\Omega_{Fe(i)}^{\gamma\rightarrow\varepsilon} = \Omega_{Fe(i)}^{\varepsilon} - \Omega_{Fe(i)}^{\gamma} \quad (4)$$

The aforementioned investigations of the regular solution model in Fe-based alloys have used a plethora of thermodynamic data for calculating the free energy and interaction parameter terms of Eq. (3) and (4). Here, the most updated [19] and commonly accepted thermodynamic data via CALPHAD review [21,22] are used which have been shown to be most applicable to a Fe-Mn-Al-Si-C system [3,12]. The

summarized literature data for $\Delta G_i^{\gamma\to\varepsilon}$ and $\Delta\Omega_{Fe(i)}^{\gamma\to\varepsilon}$ used in this investigation are reported in Table 1. The driving force for the γ→ε transformation can also be calculated directly via computational thermodynamic tools such as Thermocalc [23] which are regarded as robust models of complex alloy systems. However, the extrapolations required to calculate the Gibbs free energies at the low temperatures and high alloying atomic fractions where the γ→ε transformation occurs in Fe-Mn-X-Y-Z systems have been shown to produce grievous errors for some cases [24]. A comparison between the regular solution model and Thermocalc [23] predictions will be presented in Section 6.

Table 1. Free energy differences and interaction parameter differences between γ and ε phases. Temperature is in K.

Free Energy Difference (J/mol)			**Interaction Parameter Difference (J/mol)**		
Fe	$\Delta G^{\gamma\to\varepsilon} = -822+1.7T+2.2E-3T^2$	[19]	Fe(Fe)	---	
Mn	$\Delta G^{\gamma\to\varepsilon} = 3{,}970 - 1.666T$	[18]	Fe(Mn)	$\Delta\Omega^{\gamma\to\varepsilon} = -10{,}836 + 22{,}886X_{Mn}$	[25]
Si	$\Delta G^{\gamma\to\varepsilon} = -1{,}800 + T$	[21]	Fe(Si)	$\Delta\Omega^{\gamma\to\varepsilon} = 1{,}780$	[3]
Al	$\Delta G^{\gamma\to\varepsilon} = 5{,}481.04 - 1.799T$	[21]	Fe(Al)	$\Delta\Omega^{\gamma\to\varepsilon} = 3{,}323$	[12]
C	$\Delta G^{\gamma\to\varepsilon} = -24{,}595.12$	[12]	Fe(C)	$\Delta\Omega^{\gamma\to\varepsilon} = 42{,}500$	[26]

4. MODELING THE DRIVING FORCE OF THE γ→α' MARTENSITIC TRANSFORMATION

Direct calculation of the driving force for the second stage TRIP martensitic transformation of ε→α' is not well documented. Instead, an indirect approach is presented here where $\Delta G^{\varepsilon\to\alpha'}$ can be determined by:

$$\Delta G^{\varepsilon\to\alpha'} = \Delta G^{\gamma\to\alpha'} - \Delta G^{\gamma\to\varepsilon} \tag{5}$$

where the driving force for the γ→α' martensitic reaction, $\Delta G^{\gamma\rightarrow\alpha'}$, has been well reviewed [16,27,28]. A first attempt at calculating $\Delta G^{\gamma\rightarrow\alpha'}$ was performed by Zener [29] in which the regular solution model:

$$\Delta G^{\gamma\rightarrow\alpha'} = X_{Fe}\Delta G_{Fe}^{\gamma\rightarrow\alpha} + \sum X_i \Delta G_i^{\gamma\rightarrow\alpha} + \sum \Delta G_{Mix}^{\gamma\rightarrow\alpha'} \quad (6)$$

was simplified under the assumption of dilute, ideal solutions such that the free energy of mixing, $\Delta G_{Mix}^{\gamma\rightarrow\alpha'}$, is zero and that $RT\ln(x_\alpha / x_\gamma)$ is constant. In this regard, Eq. (6) is reduced to:

$$\Delta G^{\gamma\rightarrow\alpha'} = X_{Fe}\Delta G_{Fe}^{\gamma\rightarrow\alpha} + \sum X_i \Delta H_i^{\gamma\rightarrow\alpha'} \quad (7)$$

where $\Delta H_i^{\gamma\rightarrow\alpha'}$ is the difference in enthalpy for the solute, *i*, in the austenitic and martensitic phases. Zener's assumption of dilute solution is not considered valid for the low SFE TRIP alloys examined here that have total solute concentrations in excess of 15 at% but is presented for the discussion of possible error in subsequent models. Zener's simplifying approach was an effort to remove the activity parameter in the free energy expression in response to the limited amount of data on solute activity in solid solution. Because of the inherent difficulty in measuring solid solution activity, values in literature at present are still lacking or are only available for a minimal temperature regime.

A different approach to modeling the energy of the transformation in Fe-C-X alloys without necessitating the consideration of solute activity was derived by Aaronson, Domain, and Pound (ADP) [30] under the assumption that the change in free energy in pure iron can be separated into a non-magnetic and magnetic contribution:

$$\Delta G_{Fe}^{\gamma\rightarrow\alpha} = \Delta G_{Fe(NM)}^{\gamma\rightarrow\alpha} + \Delta G_{Fe(Mag)}^{\gamma\rightarrow\alpha} \quad (8)$$

The addition of substitutional alloying elements affects each term independently by varying the component's free energy dependence on temperature and is thus represented by the terms ΔT_{NM} and ΔT_{Mag} given per at% solute. Without activity data for interstitial C, ADP [30] described the effect of carbon in an empirical manner by comparing calculated driving force values with experimental data. The original equation described by the ADP model has been modified here for use in multi-substitutional solute systems and is thus given as:

$$\Delta G^{\gamma\to\alpha} = \left(1 - X_C\right)\begin{bmatrix} 141\sum X_i\left(\Delta T_{Mag,i} - \Delta T_{NM,i}\right) + \\ \Delta G_{Fe}^{\gamma\to\alpha}\left\{T - 100\sum X_i \Delta T_{Mag,i}\right\} \end{bmatrix} + X_C\left(k - RT\ln 3\right) \qquad (9)$$

where X_C is the mole fraction of carbon, X_i is the mole fraction of substitutional solute and k = 39,217 J/mol [30]. The calculation of $\Delta G^{\gamma\to\alpha}$ is relevant due to the diffusionless nature of the γ→α' martensitic transformation, such that value of the chemical driving force is often expressed as:

$$\Delta G^{\gamma\to\alpha'} = \Delta G^{\gamma\to\alpha} + \Delta f^{*} \qquad (10)$$

where $\Delta G^{\gamma\to\alpha}$ is the driving force for transformation from γ-austenite to α-ferrite of identical composition and Δf^* is the Zener ordering parameter that describes the change in energy associated with the spontaneous ordering of interstitial C atoms in the ferrite lattice at some ordering temperature, T_C [31]. It can be shown for the low C content of the alloys investigated in this study (0.07-0.15 wt.%) that T_C < 173K (-100°C) and as such Δf^* can be neglected for any model presented here.

Bhadeshia [32] has adopted the ADP model's magnetic substitutional solute expression and combined it with a more thorough description of carbon's interstitial role in the lattice, yielding:

$$\begin{aligned}\Delta G^{\gamma\to\alpha'} &= 2X_C RT\ln X_C + X_C\left[\Delta\bar{H}_\alpha - \Delta\bar{H}_\gamma - T\left(\Delta S_\alpha - \Delta S_\gamma\right) + 4\omega_\alpha - 6\bar{\omega}_\gamma\right] \\ &-4RT\left(1-X_C\right)\ln\left(1-X_C\right) + 5RT\left(1-2X_C\right)\ln\left(1-2X_C\right) - 6RTX_C\ln\left[\frac{\delta_\gamma - 1 + 3X_C}{\delta_\gamma + 1 - 3X_C}\right] \\ &-6RT\left(1-X_C\right)\ln\left[\frac{1-2J_\gamma + X_C\left(4J_\gamma - 1\right) - \delta_\gamma}{2J_\gamma\left(2X_C - 1\right)}\right] + 3RTX_C\ln\left(3-4X_C\right) \\ &+4RTX_C\ln\left[\frac{\delta_\alpha - 3 + 5X_C}{\delta_\alpha + 3 - 5X_C}\right] + \left(1-X_C\right)\left[\begin{matrix}141\sum Y_i\left(\Delta T_{Mag,i} - \Delta T_{NM,i}\right) + \\ \Delta G_{Fe}^{\gamma\to\alpha}\left\{T - 100\sum Y_i\Delta T_{Mag,i}\right\}\end{matrix}\right] + \Delta f^*\end{aligned} \tag{11}$$

where $Y_i = X_i/X_{Fe}$ has been substituted for X_i of Eq. (10) and where ω_γ is the carbon-carbon interaction energy in austenite and is dependent on the type and amount of substitutional elements present in solution. The averaged parameter used here, $\bar{\omega}_\gamma$, has been calculated accounting for the effects of Mn and Si according to relations derived by Bhadeshia [32,33]. For brevity, the remaining term descriptions and the values used in this investigation for all α-martensite models are listed in the appendix.

An approach is also taken here to develop a regular solution model similar to that derived for the γ→ε transformation using elemental [21] and binary [34-37] CALPHAD data and is expressed as:

$$\Delta G^{\gamma\to\alpha'} = X_{Fe}\Delta G_{Fe}^{\gamma\to\alpha} + \sum X_i\Delta G_i^{\gamma\to\alpha} + \sum X_i X_{Fe}\Delta\Omega_{Fe(i)}^{\gamma\to\alpha} \tag{12}$$

for low carbon steels where the Zener ordering parameter may again be neglected. The driving force for the γ→α (γ→α') transformation can also be calculated directly via FactSAGE [38] thermodynamic software and will be compared to the outlined models for

reference. Ultimately the desired Gibbs free energy change of the second stage TRIP transformation, $\Delta G^{\varepsilon \rightarrow \alpha'}$, can be calculated from any of these models using Eq. (5).

5. EXPERIMENTAL PROCEDURE

In addition to analyzing FeMnAlSiC steels from literature an additional alloy is presented in this study. The alloy was melted in an induction furnace under an argon atmosphere and alloying was added in the form of electrolytic manganese, pure aluminum, ferrosilicon and graphite. The alloy was calcium treated in the furnace before tapping at 1848K (1575°C) into a lip pouring ladle which was used to cast no-bake phenolic Y-block molds utilizing Foseco KALPUR exothermic riser sleeves. Y-block dimensions measured 12.6 cm x 6 cm x 1.7 cm. Castings were homogenized at 1373K (1100°C) for 2 hours and air cooled to room temperature before being milled to rectangular blocks of dimensions 13 mm x 126 mm x 50 mm. Hot rolling was performed incrementally at a starting temperature of 1223K (950°C) with reheating between reductions once the temperature approached the expected A_3 temperature near 973K (700°C). The plates were hot reduced 82% to a final hot band thickness of 2.3 mm. After the final rolling pass, the hot band was reheated to 1223 K (950°C) for 5 minutes before being water quenched to room temperature. Tensile specimens were machined from the hot rolled material according to ASTM E8-08 [39] with a gage length of 50 mm and width of 12.5 mm. Tensile testing was performed at room temperature at a displacement rate of 0.01 mm/s with the loading axis parallel to the rolling direction. Chemical analysis was performed by ion coupled plasma spectrometry after sample dissolution in hydrochloric and nitric acid. A Phillips X-pert diffractometer using Cu Kα radiation was used to quantify the microstructures of the cast and rolled material via

integrated intensity calculations of the diffraction peaks as outlined by De et al. for steels containing an ε-martensite constituent [40].

6. RESULTS AND DISCUSSION

Seven high Mn steels [2,4,6,7,41] which have exhibited TRIP behavior involving the formation of ε-martensite were analyzed using the proposed thermodynamic models. Their compositions and microstructural phases before and after tensile deformation are listed in Table 2. Calculated room temperature martensitic driving forces for the $\gamma \rightarrow \varepsilon$ transformation and associated SFE are presented in Table 3. The driving force predicted by Thermocalc [23] was typically 2-8 times greater in magnitude than that calculated by the regular solution model. Applying the value of $\Delta G^{\gamma \rightarrow \varepsilon}$ from Thermocalc [23] to the SFE equation yields negative stacking fault energies for Alloy C of Pisarik et al. [6] and for Alloy D of this study. While a negative SFE is possible, it would indicate that for all values of *n* in Eq. 1, austenite is unstable relative to ε-martensite which could nucleate from any single lattice dislocation, thereby resulting in compete transformation. However, these alloys contained 14-18% retained austenite in the room temperature microstructure and as such these results do not agree with the implications of the Thermocalc [23] prediction. Despite Thermocalc providing reasonable values of driving force for the other three alloys considered, it is proposed here that the model employed by the software may not be robust enough to ensure accurate predictions for high Mn TRIP systems, which contain significant additions of Al and Si. A similar conclusion was reached by Yang et al. [24] in their analysis of ε-martensite start (M_S^{ε}) temperatures of 328 different high Mn (>11 wt%) steels. Thermocalc predicted a positive driving force, with some calculated $\Delta G^{\gamma \rightarrow \varepsilon}$ being greater than +2,000 J/mol, at the M_S^{ε} temperature

measured via dilatometry for 93 of the 328 compositions investigated. Yang et al. [24] concluded that Thermocalc could not be used to accurately calculate driving forces for these alloys with error being substantially worse for any system with >30wt% solute.

Table 2. High Mn TRIP chemistries in weight percent and their resulting microstructural phases which were applied to the proposed thermodynamic models.

	Composition (wt pct)					Vol % Before Tensile Test			Phases After Tensile
Alloy	Mn	Si	Al	C	N	γ	ε	α′	Test
(A) McGrath et al.[2]	15.3	2.85	2.4	0.07	0.017	27	60	13	α′
(B) Van Aken et al.[4]	14.2	1.85	2.38	0.06	0.019	37	29	34	α′
(C) Pisarik et al.[6]	15.1	1.95	1.4	0.08	0.017	14	45	41	α′
(D) This study	13.9	2.07	2.01	0.09	0.012	18	64	18	α′
(E) Pisarik et al.[6]	14.3	2.97	0.89	0.16	0.022	7	75	18	ε + α′
(F) Frommeyer et al.[41]	15.8	3.00	2.9	0.02	---	48	16	36†	γ + α + α′
(G) Yang et al.[7]	21.5	0.19	---	0.24	---	93	7	0	ε + γ

†Value represents the summation of α-martensite and α-ferrite

Table 3. Calculated room temperature driving force for the γ→ε transformation and associated SFE (n=2).

	Regular Solution Model		Thermocalc [23]	
Alloy	$\Delta G^{\gamma\rightarrow\varepsilon}$ (J/mol)	SFE (mJ/m^2)	$\Delta G^{\gamma\rightarrow\varepsilon}$ (J/mol)	SFE (mJ/m^2)
(A) McGrath et al.[2]	-42	17.6	-358	6.4
(B) Van Aken et al.[4]	-67	16.1	-432	5.2
(C) Pisarik et al.[6]	-209	7.7	-397	-0.9
(D) This study	-116	13.2	-398	-1.0
(E) Pisarik et al.[6]	-255	5.0	-279	6.0
(F) Frommeyer et al.[41]	27	21.6	---	---
(G) Yang et al.[7]	-236	6.1	---	---

The regular solution model presented here has calculated favorable driving forces for the γ→ε transformation for all of the alloys except the composition of Frommeyer et al. [41] which has a value of +27 J/mol and an associated SFE of 21.6 mJ/m^2. The error may be attributed to the duplex nature of the steel and the presence of free ferrite in the microstructure such that the bulk composition does not accurately reflect the composition of the austenite which is transforming to ε-martensite having a composition where $\Delta G^{\gamma\rightarrow\varepsilon} < 0$. Regardless, the microstructure observed by Frommeyer et al. contained the least amount of ε-martensite and greatest amount of retained austenite out of the 15wt% Mn steels examined here. Thus, the steel might be expected to have a SFE near 20 mJ/m^2 where only rare instances of extremely large thicknesses of appropriately stacking dislocations have energetic favorability to produce the γ→ε transformation. With this aspect considered, the SFE calculated from the regular solution model's driving force predictions for each alloy agree well with the reported microstructure. Figure 2 exhibits the expected linear trend of austenite stability on SFE.

It has been shown that the propensity to transform austenite to ε-martensite is dependent on the thickness, *n*, of a nucleating lattice defect in which *n*/2 dislocations must be present on every other $\{111\}_\gamma$ plane. We might expect there to be some distribution of *n* such that lower values (i.e. thinner stacking defects) are more statistically probable to be present in the microstructure. At room temperature, alloys with SFE near 20 mJ/m^2 will have few available thick defects required for nucleation and thus the amount of transformation of austenite to ε-martensite will be minimal. Those alloys with lower SFE will have a greater number of smaller, operable nucleating defects and the γ→ε transformation should be more complete. This phenomenon is depicted by

the calculated SFE as a function of *n* for the alloy of McGrath et al. [2] shown in Figure 3. With a high SFE (*n* = 2) of 17.6 mJ/m^2 at room temperature, only nucleating defects of *n* > 20 (i.e. > 10 dislocations stacked on every other close packed plane) have a SFE < 0 such that the perfect a/2<110> lattice dislocations are dissociated into infinitely wide Shockley partial dislocations of the type a/6<112> responsible for the creation of ε-martensite. The limited instances of this type of lattice defect arrangement result in a smaller fraction of ε-martensite transformed and thus a greater retention of austenite in the room temperature microstructure.

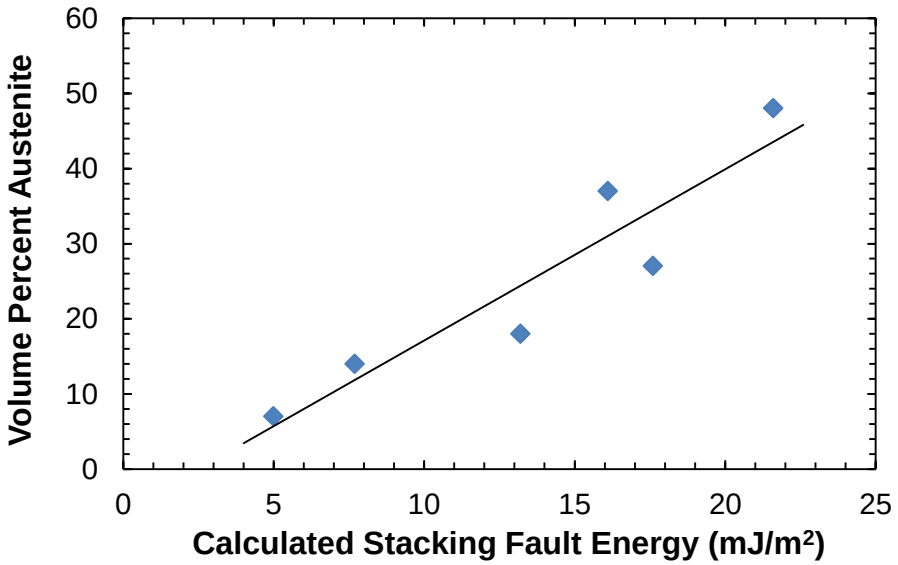

Figure 2. Correlation between calculated stacking fault energy derived from regular solution model driving forces for six 15% Mn TRIP steels and the measured percent of untransformed austenite.

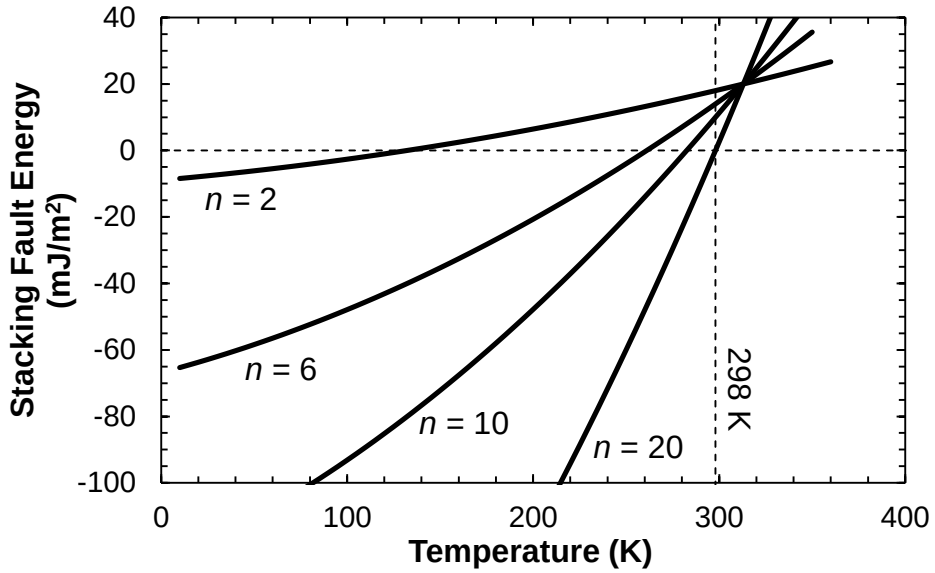

Figure 3. The effect of fault thickness on the calculated stacking fault energy for Fe-15.3Mn-2.85Si-2.4Al-0.07C-0.017N (McGrath et al. [2]). The γ→ε transformation will occur for lattice defects greater than 10 dislocations stacked on every other close packed plane.

The extent of ε-martensite formation may therefore not be a function of driving force directly but more a function of dislocation density and their physical configuration, or perhaps more appropriately, material process history. In the examination of 328 alloys and measured M_S^{ε} temperatures reported in literature, Yang et al. [24] revealed no correlation between M_S^{ε} temperature and driving force as calculated using Thermocalc. What has not been considered is the dilatometry technique (e.g. heating rate, peak temperature and peak hold time, etc.) which may have influenced the dislocation substructure before quenching thereby altering the distribution of the critical fault thickness, n^*, associated with an observed M_S^{ε} temperature. Olson and Cohen [11] have proposed that a finite symmetric tilt boundary segment in which the dislocations have a periodic arrangement analogous to every other $\{111\}_{\gamma}$ plane could serve as a source for

thick nucleating defects. However, such a dislocation arrangement would represent a high energy defect and likely experience high climb forces. As such, one might expect nucleating defects of this character to decompose during high temperature anneals. This conclusion can be supported by considering the process history of the alloys presented here. The alloy from this study, along with McGrath et al. [2], Van Aken et al [4], and Pisarik et al. [6] were hot rolled in plate form to final thickness and reheated at 900 to 950°C for 5 minutes before water quenching. The high percentage of ε-martensite (>29%) in these alloys may be a result of incomplete recovery of lattice defects induced upon rolling. In contrast, the material prepared by Yang [7] was annealed at 1100°C for 4 hours and oil quenched. The elimination of large nucleating defects during annealing may explain why Yang et al.'s alloy exhibits the lowest percentage of ε-martensite (3%) despite having a significant driving force of -236 J/mol and a low calculated SFE of 6.1 mJ/m^2.

Calculated values of the chemical driving force for the γ→α' transformation at room temperature from the five investigated models are listed in Table 4. All models are consistent in regard to the magnitude of calculated driving force of one alloy relative to another in the same model. As such, no differentiating conclusions based upon the comparison of measured microstructural phases to magnitudes of driving force can be drawn to confirm the validity of one model over another. However, analyzing the composition of Yang et al. [7] reveals some discrepancy between the models in predicting favorability of the γ→α' transformation in which the regular solution model, the Zener [29] model, and FactSage [38] all favor the reaction. Yang et al. [7] did not report any presence of α-martensite either in the annealed or deformed microstructure.

Calculated here is only the chemical driving force contribution to the phase transformation which is balanced by nonchemical effects such as interfacial and strain energy as predicted by general nucleation theory. Cohen et al. [43] have estimated the total amount of this energy to be approximately 272 J/mol. This inhibiting energy might be enough to compensate for the -356 J/mol chemical driving force predicted by the regular solution model and therefore it is left as a viable model. The Zener [29] model suggests a strong driving force of -1495 J/mol and is considered to be erroneous. It is likely that the large error stems from Zener's simplifying assumption of ideal solution behavior which cannot be applied to the >15% solute system's investigated here. While the FactSage [38] prediction of $\Delta G^{\gamma \rightarrow \alpha}$ = -660 J/mol is more reasonable than that of the Zener model, this value cannot be adequately equated to a counteracting nucleation energy and is therefore, too, considered erroneous for these alloy rich compositions. A graphical depiction of each model's dependence on temperature is shown in Figure 4 for the alloy of McGrath et al. [2]. For each 15%Mn alloy, the Zener [29] model and FactSage [38] calculation lie in close proximity confirming they are of equal error and as such will not be considered further.

Table 4. Calculated room temperature chemical driving force for the γ→α' transformation.

	Room Temperature $\Delta G^{\gamma\rightarrow\alpha'}$ (J/mol)				
Alloy	Reg. Soln.	Zener[29]	ADP[30]	Bhadeshia[32]	FactSage[38]
(A) McGrath et al.[2]	-1478	-2724	-1107	-294	-2655
(B) Van Aken et al.[4]	-1767	-2949	-1374	-600	-2822
(C) Pisarik et al.[6]	-1593	-2751	-986	-175	-2458
(D) This study	-1758	-2940	-1347	-545	-2795
(E) Pisarik et al.[6]	-1515	-2697	-967	-40	-2546
(F) Frommeyer et al.[41]	-1480	-2753	-1146	-405	-2767
(G) Yang et al.[7]	-356	-1495	372	1042	-660

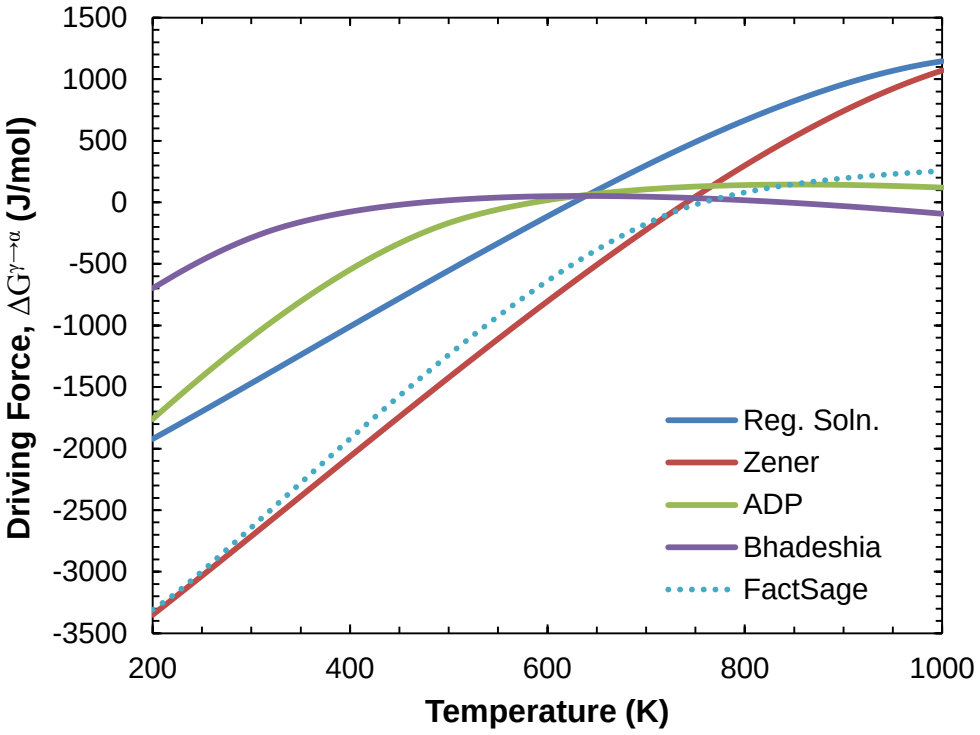

Figure 4. The temperature dependence of calculated driving forces of the γ→α' transformation by five thermodynamic models.

The ADP [30] model and Bhadeshia [32] model are both derived from the separation of the magnetic and non-magnetic contributions to the overall γ→α driving force of pure iron. However, the models differ quite significantly in their handling of the contribution of solute. The values of ΔT_{NM} and ΔT_{Mag} used in these equations for any substitutional alloying element are derived per at% of that element in binary solution with Fe. The ADP [30] model has been altered here in an attempt to account for multi-substitutional element alloys by including the summation of the effect of each individual element which is left calculated per atomic fraction, X_i. Bhadeshia's adaptation of the calculation accounts for the dilution of the Fe matrix by the addition of substitutional alloys such that the effect of each individual elements is calculated per a normalized atomic fraction, Y_i ($=X_i/X_{Fe}$). With solute concentrations on the order of 15-20 at% in these alloys, the change in calculated driving force is severe, as shown graphically in Figure 4. When recalculated using Y_i, the ADP [30] model nearly converges with the Bhadeshia [32] model save for the small differences (~50-100 J/mol) induced by Bhadeshia's more accurate handling of the effect of C. Thus, the correctness of either of these models is dependent on the appropriate handling of the magnitude of the effect for solute additions. The Bhadeshia [32] model calculates chemical driving forces of -175, -40, and -294 J/mol for the alloys of Pisarik et al. [6] (C and E) and McGrath et al. [2], respectively. With the consideration of the 272 J/mol strain and surface energy barrier to nucleation discussed earlier, the γ→α' transformation loses predicted favorability as calculated by this model. However, Pisarik et al. [6] found α-martensite nucleated from both the γ→α' and the ε→α' transformation mechanisms in Alloy C via electron backscattered diffraction characterization. Therefore, it becomes apparent that the atomic

fraction normalization technique utilized by the Bhadeshia [32] model may overestimate the effect of high solute additions and thus not be applicable for high Mn TRIP alloy systems. While the ADP [30] model's use of X_i instead of Y_i may be more appropriate, there is still a question as to the valid compositional ranges that the constant values of ΔT_{NM} and ΔT_{Mag} apply. The values used here were calculated by Zener [44] and Aaronson et. al. [27] and correspond to the ΔT required to explain the observed $\Delta M_S^{\alpha'}$ per at.% solute as determined for the limiting composition of the gamma-loop for alpha stabilizers. This corresponds to 1.8 wt% in the Fe-Si system and 1.0 wt% in the Fe-Al system and suggests that extrapolation to greater solute concentrations may not be reasonable. Thus, the regular solution model derived here (Eq. 12) likely gives the best approximation of $\Delta G^{\gamma\rightarrow\alpha'}$ for the FeMnAlSiC steels investigated here. Each alloying constituent has a fractional contribution to the total driving force based upon its own pure substance driving force for the $\gamma\rightarrow\alpha$ transformation. Substitutional and interstitial interaction effects in an Fe matrix are considered in the form of the interaction parameter, $\Delta\Omega^{\gamma\rightarrow\alpha}$, which is based upon the binary Fe-X system and is relevant for any concentration. Using a regular solution model for the calculation of $\Delta G^{\gamma\rightarrow\alpha'}$ is also advantageous when considering the calculation of $\Delta G^{\gamma\rightarrow\varepsilon}$ has also been performed here using a regular solution model. Therefore the calculation of $\Delta G^{\varepsilon\rightarrow\alpha'}$ should ensure thermodynamic data source continuity.

With both models now established, the driving force predictions, including $\Delta G^{\varepsilon\rightarrow\alpha'}$, are presented in Table 5. The formation of α-martensite from ε-martensite, from a chemical energy perspective, is predicted favorable for all the steels investigated. The steel of Yang et al. [7] has a calculated $\Delta G^{\varepsilon\rightarrow\alpha'}$ of -120 J/mol which should be adequately

balanced by a counteracting strain and interfacial energy comparable to the 272 J/mol previously reported for the γ→α' transformation such that the barrier to nucleation is not overcome thus supporting the lack of observed α-martensite in the annealed and deformed structures. There should also exist some critical thickness of an α-martensite embryo analogous to that discussed for ε-martensite nucleation. Olson and Cohen [45] have estimated the critical thickness to be on the order of 13.5 close packed planes whereas up to 27 planes has been suggested necessary by Staudhammer et al. [46]. Under the HCP→BCC nucleation mechanism proposed by Olson and Cohen [47], this would require at least one ε-martensite band of 7 to 14 dislocations in thickness to produce an α-martensite nucleus. Under previous reasoning, if the annealing treatment performed by Yang et al. [7] was sufficient to remove large nucleating lattice defects, the formation of ε-martensite, and subsequent α-martensite will be suppressed. This explanation applies to the pre-tensile microstructure observed by Yang et al. [7] but it should be expected that tensile deformation would produce an adequate amount of shear on $\{111\}_\gamma$ slip planes to make the ε→α' possible and thus the lack of α-martensite in the post-tensile microstructure must be attributed to the proposed strain and interfacial energy barrier.

Table 5. Calculated driving forces for the γ→ε and ε→α' transformations in FeMnAlSiC steels.

Alloy	SFE (mJ/m^2)	$\Delta G^{\gamma\rightarrow\varepsilon}$ (J/mol)	$\Delta G^{\varepsilon\rightarrow\alpha'}$ (J/mol)	Vol % Before Tensile Test γ	ε	α′	Phases Present After Tensile Test
(A) McGrath et al.[2]	17.6	-42	-1436	27	60	13	α′
(B) Van Aken et al.[4]	16.1	-67	-1700	37	29	34	α′
(C) Pisarik et al.[6]	7.7	-209	-1384	14	45	41	α′
(D) This study	13.2	-116	-1642	18	64	18	α′
(E) Pisarik et al.[6]	5.0	-255	-1260	7	75	18	ε + α′
(F) Frommeyer et al.[41]	21.6	27	-1507	48	16	36†	γ + α + α′
(G) Yang et al.[7]	6.1	-236	-120	93	7	0	ε + γ

†Value represents the summation of α-martensite and α-ferrite

Of the 15wt% Mn steels, the Fe-14.3Mn-2.97Si-0.89Al-0.16C alloy (Alloy E) studied by Pisarik et al. [6] has the highest calculated driving force for the γ→ε transformation (-255 J/mol) and lowest calculated driving force for the ε→α' transformation (-1260 J/mol). The alloy had the largest reported fraction of ε-martensite in the pre-tensile condition of the steels presented here. Pisarik et al. [6] reported Alloy E exhibited limited ductility and failed prematurely at 11% elongation and 726 MPa resulting in a post-tensile microstructure of ε- and α-martensite. The authors' conclusion that the incomplete ε→α' transformation was a result of over-stabilized ε-martensite is supported here by the calculated driving forces ($\Delta G^{\varepsilon\rightarrow\alpha'}$) being approximately 100 to 400 J/mol less than similar alloys which exhibited complete transformation to α-martensite upon tensile deformation. Comparison of the magnitude of $\Delta G^{\varepsilon\rightarrow\alpha'}$ for the alloys of McGrath et al. [2] and Van Aken et al. [4] also yields an explanation for the differing amount of α-martensite in the pre-tensile microstructure. The alloys have approximately the same stability of ε-martensite in reference to austenite (i.e. $\Delta G^{\gamma\rightarrow\varepsilon}$) but the alloy of

Van Aken et al. [4] exhibits an additional (-)264 J/mol free energy change for the secondary transformation of ε→α' and as such exhibits more than twice the amount of α-martensite.

Of final consideration should be the effect of chemical inhomogeneity on the local favorability of the γ→ε→α' transformation. McGrath et al. [2] used Scheil modeling to determine the chemistry of the last 15% liquid to solidify in their alloy as Fe-22.3Mn-5Si-1.3Al-0.25C in comparison to the bulk chemistry of Fe-15.3Mn-2.85Si-2.4Al-0.07C. The solidification segregation was confirmed via qualitative SEM/EDS analysis and these solute rich regions were shown to be the last regions of the microstructure to undergo the TRIP phenomenon during tensile deformation. Using the thermodynamic model presented here, the calculated driving force for the segregated regions is $\Delta G^{\gamma\rightarrow\varepsilon} = 1$ J/mol and $\Delta G^{\varepsilon\rightarrow\alpha'} = 0$ J/mol. Based on previous nucleation barrier reasoning, this would suggest the alloy of McGrath et al. [2] should not have exhibited complete transformation to α-martensite; however at tensile elongations of 20-30 pct, it is likely there existed sufficient dislocations and shear stress to initiate the transformation. It is certainly evident, however, that the chemical segregation can significantly influence the driving force of the γ→ε→α' transformation. An increase in SFE as calculated from $\Delta G^{\gamma\rightarrow\varepsilon}$ has been shown to require a large nucleating defect, *n*, to form ε-martensite. In the same regard, a higher SFE is expected to require higher stress for transformation [14,48], and thus delay the transformation to higher strains. As such, both bulk and segregated chemistries must be considered when predicting the nature of the two-stage TRIP progression during tensile deformation.

7. CONCLUSIONS

A review of thermodynamic models for the prediction of driving force for the γ→ε, γ→α', and subsequent ε→α' martensitic transformations for high Mn TRIP composition has been investigated. The Thermocalc [23] software package overestimated the γ→ε driving force while the regular solution model provided excellent agreement between calculated stacking fault energy and the measured retained austenite fraction. The role of available nucleating defects of critical size, n^*, has been linked to the SFE necessary to observe the γ→ε transformation and it is thus proposed that the amount of ε-martensite in the observed microstructures is a function of material processing history as well as thermodynamic driving force. Five models were compared for the calculation of γ→α' transformation driving force. The Zener [29] model incorrectly predicted favorable α-martensite formation ($\Delta G^{\gamma\rightarrow\alpha'}$ = -1495 J/mol) in the alloy of Yang et al. [7] and is attributed to the model's assumption of ideal solution behavior. The FactSage [38] software package calculated similar driving force magnitudes to those of the Zener [29] model and is concluded to be incapable of accurately predicting the high solute systems of FeMnAlSiC TRIP systems. The Bhadeshia [32] model has predicted values 2-3 times less than the similar the Aaronson, Domain, and Pound [30] model adopted here for multi-substitutional alloys. The deviation is related to the treatment of the contribution of substitutional elements on the driving force as proportional to a molar fraction normalized to iron content. It is concluded that both models are not applicable for alloys with Si and Al contents greater than 1.8wt% and 1.0 wt% respectively as these represent the limit to which the utilized ΔT parameters may be valid. The regular solution model has calculated reasonable values of $\Delta G^{\gamma\rightarrow\alpha'}$ which have been used to further calculate

$\Delta G^{\varepsilon \rightarrow \alpha'}$. The predicted driving forces for transformation correspond well with the microstructure and behavior of the seven FeMnAlSiC steels from literature compared here when considered in conjunction with the role of strain and interface nucleation energy, nucleating defect critical size, and material process history. The developed regular solution models can therefore be used as a thermodynamic tool in the prediction of the $\gamma \rightarrow \varepsilon \rightarrow \alpha'$ martensitic transformation and the resulting microstructural constituents and may give some indication to the nature of two-stage TRIP behavior upon deformation if the extent of solute segregation is well understood.

ACKNOWLEDGEMENTS

This work was supported by the Peaslee Steel Manufacturing Research Center (PSMRC). The authors gratefully acknowledge Jerry Arnold of AK Steel Corporation for his assistance with Thermocalc calculations.

APPENDIX

All $\Delta G^{\gamma\rightarrow\alpha'}$ models utilized Eq (A.1) taken from SGTE [21] for the value of $\Delta G_{Fe}^{\gamma\rightarrow\alpha}$ which accounts for magnetic contribution to the free energy change:

$$\Delta G_{Fe}^{\gamma\rightarrow\alpha} = 1462.4 - 8.282 + 1.15T\ln T - 6.4\times10^{-4}T^2 + G_{mag}^{\alpha} + G_{mag}^{\gamma} \quad \text{(A.1)}$$

where G_{mag} can calculated as described in Ref. [21].

Table A.1. Values of $\Delta H_i^{\gamma\rightarrow\alpha'}$ utilized in the Zener model [29]. The value for Mn was taken as the average of the two listed.

Binary Component	$\Delta H_i^{\gamma\rightarrow\alpha'}$ (J/mol)	Reference
C	33,890.4	[29]
N	22,426.2	[29]
Mn	10,209.0	[29]
Mn	11,296.8	[49]
Al	-5,439.2	[29]
Si	-1,987.4	[29]

Table A.2. Thermodynamic values utilized in the ADP model [30].

Binary Component	ΔT_{Mag} (per at.%)	ΔT_{NM} (per at.%)	Reference
Mn	-37.5	-39.5	[30]
Al	8	15	[30]
Si	-3	0	[30]

The Bhadeshia model [32] requires the calculation of four parameters as given by Eq. (A.2-A.5):

$$\delta_\alpha = \sqrt{9 - 6X_C\left(2J_\alpha + 3\right) + X_C{}^2\left(9 + 16J_\alpha\right)} \quad \text{(A.2)}$$

$$\delta_\gamma = \sqrt{1 - 2X_C\left(1 + 2J_\gamma\right) + X_C{}^2\left(1 + 8J_\gamma\right)} \quad \text{(A.3)}$$

$$J_\alpha = 1 - e^{-\omega_\alpha/RT} \quad \text{(A.4)}$$

$$J_\gamma = 1 - e^{-\bar{\omega}_\gamma / RT} \tag{A.5}$$

Table A.3. Thermodynamic values utilized in the Bhadeshia model [32].

Parameter	Value	Units	Reference
$\Delta\bar{H}_\alpha$	111,918	J/mol	[50]
$\Delta\bar{H}_\gamma$	38,575	J/mol	[33]
ΔS_α	51.44	J/mol·K	[50]
ΔS_γ	13.48	J/mol·K	[33]
ω_α	48,570	J/mol	[32]

Table A.4. References for free energy differences and interaction parameter differences between γ and α phases utilized in the regular solution model.

Free Energy Difference Ref.		Interaction Parameter Difference Ref.	
Fe	Dinsdale [21]		
Mn	Dinsdale [21]	Fe(Mn)	Kaufman [37]
Si	Dinsdale [21]	Fe(Si)	Kaufman [35]
Al	Dinsdale [21]	Fe(Al)	Kaufman [36]
C	Kaufman [34]	Fe(C)	Kaufman [34]

REFERENCES

[1] J. Fekete and J. Hall: NIST Internal Report 6668, National Institute of Standards and Technology, Washington, DC, May 2012.

[2] M.C. McGrath, D.C. Van Aken, N.I. Medvedeva, and J.E. Medvedeva: *Metall. Mater. Trans. A*, 2013, vol. 44A, pp. 4634-43.

[3] O. Grässel, G. Frommeyer, C. Derder, and H. Hofmann: *J.Phys. IV France*, 1997, vol. 7, pp. C5-383-88.

[4] D.C. Van Aken, S.T. Pisarik, and M.C. McGrath: *Proc. Intl. Symp. Develop. AHSS*, 2013, Vail, Colorado, pp. 119-129.

[5] L. Bracke, L. Kestens, and J. Penning: *Scripta Mater.*, 2007, vol. 57, pp. 385–88.

[6] S.T. Pisarik, D.C. Van Aken, K. Limmer, and J. Medvedeva: *Proc. of AISTech 2014*, 2014, pp. 3013-23.

[7] E.Yang, H. Zurob, and J. McDermid: *Proc. of MS&T'10*, 2010, pp. 1914-25.

[8] S. Takaki, T. Furuya, and Y. Tokunaga: *ISIJ Int.*, 1990, vol. 30, pp. 632-38.

[9] M. Koyama, T. Sawaguchi, and K. Tsuzaki: *Metall. Mater. Trans. A*, 2012, vol. 43, pp. 4063-74.

[10] S. Kibey, J. Liu, M. Curtis, D. Johnson, and H. Sehitoglu: *Acta Mater.*, 2006, vol. 54, pp. 2991-3001.

[11] G. Olson and M. Cohen: *Metall. Mater. Trans. A*, 1976, vol. 7, pp. 1897-1904.

[12] W.S. Yang and C.M Wan: *J. Mater. Sci.*, 1990, vol. 25, pp. 1821-23.

[13] P.J. Ferreira and P. Mullner: *Acta Mater.*, 1998, vol. 46, pp. 4479-84.

[14] J. Talonen and H. Hänninen: *Acta Mater.*, 2007, vol. 55, pp. 6108-18.

[15] H. Fujita and S. Ueda: *Acta Metall.*, 1972, vol. 20, pp. 759-67.

[16] L. Kaufman and M. Cohen: *Progr. Metal. Phys.*, 1958, vol. 7, pp. 165-246.

[17] A. Dumay, J.P. Chateau, S. Allain, S. Migot, and O. Bouaziz: *Mater. Sci. Eng. A*, 2008, vols. 483-484, pp. 184-87.

[18] J.F. Breedis and L. Kaufman: *Metall. Trans.*, 1971, vol. 2, pp. 2359-71.

[19] Y.K. Lee and C.S. Choi: *Metall. Mater. Trans. A*, 2000, vol. 31, pp. 355-60.

[20] S. Allain, J.P. Chateau, O. Bouaziz, S. Migot, N. Guelton: *Mater. Sci. Eng. A*, 2004, vols. 387-389, pp.158-62.

[21] A.T. Dinsdale: *CALPHAD*, 1991, vol. 15, pp. 317-425.

[22] L. Kaufman, *CALPHAD*, 1977, vol. 1, pp. 7-89.

[23] B. Sundman, B. Jansson, and J.O. Anderson: *CALPHAD*, 1985, vol. 9, pp. 153-190.

[24] H.S. Yang, J.H. Jang, H.K.D.H. Bhadeshia, and D.W. Suh: *CALPHAD*, 2012, vol. 36, pp. 16-22.

[25] K. Ishida and T. Nishizawa: *Trans. Jpn. Inst. Met.*, 1974, vol. 15, pp. 225-231.

[26] P.H. Adler, G.B. Olson, and W.S. Owen: *Metall. Trans. A*, 1986, vol. 16A, pp. 1725-37.

[27] H. I. Aaronson, M. Enomoto, and J.K. Lee: *Mechanisms of Diffusional Phase Transformations in Metals and Alloys*, 1st ed., CRC Press, Boca Raton, FL, 2010, 99. 608-13.

[28] H.K.D.H. Bhadeshia and R.W.K. Honeycombe: *Steels: Microstructure and Properties*, 3rd ed., Elsevier, Amsterdam, 2006, pp. 116-18.

[29] C. Zener: *Trans. Am. Inst. Min. (Metall.) Eng. AIME*, 1946, vol. 167, pp. 513-34.

[30] H.I. Aaronson, H.A. Domain, and G.M. Pound: *Trans. Metall. Soc. AIME*, 1966, vol. 236, pp. 768-81.

[31] C. Zener: *Trans. Am. Inst. Min. (Metall.) Eng. AIME*, 1946, vol. 167, pp. 550-95.

[32] H.K.D.H. Bhadeshia: *Metal Sci.*, 1981, vol. 15, pp. 178-180.

[33] H.K.D.H. Bhadeshia, Program MAP_STEEL_MUCG46, Materials Algorithms Project Program Library, University of Cambridge: http://www.msm.cam.ac.uk/map/steel/programs/mucg46-b.html.

[34] L. Kaufman: *CALPHAD*, 1978, vol. 2, pp. 295-318.

[35] L. Kaufman: *CALPAHD*, 1979, vol. 3, pp. 45-76.

[36] L. Kaufman: *CALPHAD*, 1978, vol. 2, pp. 325-48.

[37] L. Kaufman: *CALPHAD*, 1978, vol. 2, pp. 117-46.

[38] Thermfact and FTT-Technologies, FactSage 6.2, Aachen, Germany, 2009.

[39] ASTM E 8/E 8M-08, Standard Test Methods for Tension Testing of Metallic Materials.

[40] A.K. De, D.C. Murdock, M.C. Mataya, J.G. Speer, and D.K. Matlock: *Scr. Mater.*, 2004, vol. 50, pp. 1445-49.

[41] G. Frommeyer, U. Brux, and P. Neumann: *ISIJ Int.*, 2003, vol. 3, pp. 438-46.

[42] H.S. Yang, J.H. Jang, H.K.D.H. Bhadeshia, and D.W. Suh: *CALPHAD*, 2012, vol. 36, pp. 16-22.

[43] M. Cohen, E.S. Machlin, and V.G. Paranjpe: *Thermodynamics in Physical Metallurgy*, 1st ed., American Society of Metals, Cleveland, OH, 1950, p. 242.

[44] C. Zener: *Trans. Am. Inst. Min. (Metall.) Eng. AIME*, 1955, vol. 203, pp. 619-30.

[45] G.B. Olson and M. Cohen: *Metall. Trans. A*, 1975, vol. 7A, pp. 1905-14.

[46] K.P Staudhammer, L.E. Murr, and S.S Hecker: *Acta Metall.*, 1983, vol. 31, pp. 267-74.

[47] G.B. Olson and M. Cohen: *J. Less-Common Met.*, 1972, vol. 28, pp. 107-18.

[48] T.S. Byun: *Acta Mater.*, 2003, vol. 51, pp. 3063-71.

[49] F.W Jones and W.I Pumphrey: *J. Iron Steel Inst.*, 1949, vol. 163, pp. 121-31.

[50] J.A. Lobo and G.H. Geiger: *Metall. Trans. A.*, 1976, vol. 7A, pp. 1347-57.

II. CRYSTALLOGRAPHIC ORIENTATION OF THE ε→α' MARTENSITIC (ATHERMAL) TRANSFORMATION IN A FeMnAlSi STEEL

S.T. Pisarik and D.C. Van Aken

Department of Materials Science and Engineering

Missouri University of Science and Technology

223 McNutt Hall, 1400 N. Bishop, Rolla, MO 65409-0330, USA

Tel.: 573-341-4717

Email: dcva@mst.edu

Published in Metallurgical and Materials Transactions A, volume 45A, June 2014.

Published first online, 19 April 2014

ABSTRACT

The presence of athermal ε- and α- martensite (α') in the as-cast structure of a Fe-0.08C-1.95Si-15.1Mn-1.4Al-0.017N alloy has been revealed by electron backscatter diffraction analysis. The alloy exhibited two athermal martensitic transformations described by γ→α' and γ→ε→α'. The Shoji-Nishiyama orientation relationship was observed between γ-austenite and ε-martensite while α-martensite nucleated from γ-austenite exhibited a Kurdjumov-Sachs orientation relationship. Six crystallographic variants of α-martensite consisting of three twin-related variant pairs were observed in ε-bands. A planar parallelism of $\{0001\}\varepsilon \parallel \{110\}\alpha'$ and a directional relation of $<1\bar{1}1>\alpha'$ lying within 1° of $<\bar{1}2\bar{1}0>\varepsilon$ existed for these variants.

1. INTRODUCTION

Martensitic transformations involving the ε-martensite phase have been well studied in austenitic stainless steel systems where the γ→ε→α' transformation occurs during deformation at cryogenic [1-3] or room [46] temperatures. Such transformations are typically classified as stress-induced martensitic transformations where dislocation glide and shear band intersection resulting from plastic yielding create martensite nucleation sites [5,7]. Stress-induced nucleation of martensite is the predominant phenomena in steels which exhibit Transformation Induced Plasticity (TRIP). Formation of ε-martensite during TRIP is dependent on the stacking fault energy (SFE) which can be calculated by:

$$SFE = 2\rho\Delta G^{\gamma\rightarrow\varepsilon} + 2\sigma^{\gamma/\varepsilon} \quad (1)$$

where ρ is the planar atomic density of $\{111\}\gamma$, $\Delta G^{\gamma\rightarrow\varepsilon}$ is the Gibbs free energy difference between γ-austenite and ε-martensite and $\sigma^{\gamma/\varepsilon}$ is the interfacial energy between the same

phases [8]. Alloys with SFE < 20 mJ/m^2 often exhibit a two-stage TRIP character ($\gamma \rightarrow \varepsilon \rightarrow \alpha'$) where ε-martensite acts as an intermediate phase [9]. The application of a high deforming stress in conjunction with low SFE aids to destabilize perfect a/2<110> dislocations into Shockley partial dislocations of the type a/6<112> responsible for the creation of wide stacking faults and subsequent ε-martensite bands [6,10].

In contrast to strain-induced martensitic transformation, Fe-17Mn-C [11,12] and Fe-20Mn [1] alloys have exhibited athermal ε- and α- martensite transformation upon cooling to near room temperature in the former and to 77K (-196°C) in the latter. Athermal transformations are associated with alloys which have calculated SFE ≤ 0 mJ/m^2 at some temperature in the cooling process where the thermodynamic driving force is greater than the resisting surface energy component in Eq (1). In this instance, the formation and widening of stacking faults defined by Shockley partial dislocations on every other $\{111\}_\gamma$ is favorable and a hexagonal close packed ε-martensite embryo is formed [6,10]. Recently, McGrath et al. reported exceptional tensile properties of 1165 MPa ultimate tensile strength (UTS) at 35 pct elongation to failure in a Fe-0.07C-2.85Si-15.3Mn-2.4Al-0.017N steel where a triplex microstructure containing γ-austenite, ε-martensite, and α-martensite was formed upon water quenching to room temperature after hot rolling [13]. The predominant strengthening mechanism was attributed to a two-stage TRIP phenomena characterized by the $\gamma \rightarrow \varepsilon \rightarrow \alpha'$ martensitic transformation. The low stacking fault energy (7.5 mJ/m^2) of the alloy allowed for ε-martensite formation in the as-quenched state via either an athermal process or quenching stress-assisted nucleation while also promoting strain-induced martensitic transformation during deformation. TRIP alloys similar to the one investigated by McGrath et al. show promise in fulfilling

the target properties of 1000 MPa UTS at 30 pct elongation and 1500 MPa UTS at 20 pct elongation for 3rd generation advanced high strength steels [14]. In this communication we investigate the nature of athermal α-martensite nucleated within ε-martensite in a Fe-0.08C-1.95Si-15.1Mn-1.4Al-0.017N steel in the as-cast state, since the large grain structure facilitated the analysis.

2. EXPERIMENTAL PROCEDURE

The Fe-0.08C-1.95Si-15.1Mn-1.4Al-0.017N steel was melted in an induction furnace under an argon atmosphere and alloying was added in the form of electrolytic manganese, pure aluminum, ferrosilicon, and graphite. The steel was treated with mischmetal prior to tapping at 1758K (1485°C) into a ladle bearing calcium treatment. Plates were cast at 1698K (1425°C) into a no-bake phenolic mold utilizing a Foseco KALPUR exothermic riser sleeve and graphite filter. Cast plate dimensions measured 35.5 cm x 35.5 cm x 2.0 cm. Chemical analysis was performed by ion coupled plasma spectrometry after sample dissolution in hydrochloric and nitric acid. X-ray diffraction was performed with a Phillips X-pert diffractometer using Cu Kα radiation. Phase quantification was calculated from the integrated intensity of the diffraction peaks as outlined by De et al. for steels containing an ε-martensite constituent [15]. Electron backscattered diffraction (EBSD) specimens were prepared by mechanical grinding, diamond polishing, and final vibratory polishing with 0.02 μm colloidal silica. Orientation image mapping via electron backscatter pattern analysis was performed on a Helios Nanolab 600 using a Nordlys detector and the HKL Channel5 software package. The electron beam was operated at an accelerating voltage of 30 kV and an emission current of 11 nA with a step size of 0.1 μm during mapping. A user-defined crystal

definition for ε-martensite (space group: $P6_3/mmc$, a=2.540 Å, c=4.111 Å) was constructed based upon lattice parameter analysis from XRD results and were comparable to those calculated by Martin et al. via refined Reitveld XRD peak analysis of ε-martensite in a Fe-16Cr-6.8Mn-6.1Ni steel [16].

3. RESULTS

The Fe-0.08C-1.95Si-15.1Mn-1.4Al-0.017N steel used in this study was designed with a negative calculated SFE at room temperature (-2.2 mJ/m^2) so that athermal ε-martensite formation would be possible in the as-cast structure. Phase identification from XRD analysis is shown in Figure 1. The presence of ε-martensite is denoted by two observed reflections with retained austenite and α-martensite also being detected. The as-cast structure contained on average 43 pct ε-martensite, 54 pct α-martensite, and 3 pct austenite by volume. The triplex microstructure is comparable to that observed by McGrath et al. in a hot rolled alloy of similar composition Fe-0.07C-2.85Si-15.3Mn-2.4Al-0.017N which also exhibited low calculated SFE (7.5 mJ/m^2) [13].

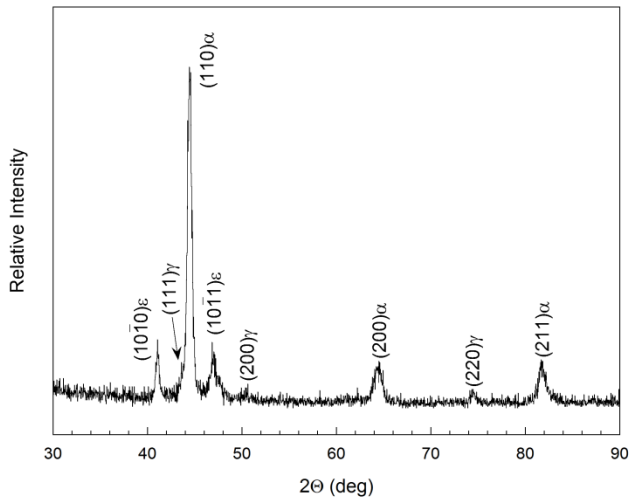

Figure 1. X-ray diffraction pattern of as-cast Fe-0.08C-1.95Si-15.1Mn-1.4Al-0.017N shows the presence of ε-martensite, α-martensite, and γ-austenite.

Figure 2 shows the results of EBSD phase characterization. The band contrast map shown in Figure 2(a) assigns a grey value to each pixel of analysis based upon Kikuchi band contrast which is affected by local dislocation density and lattice defects. As such, grain boundaries and heavily dislocated areas appear dark and the image functions much the same as a secondary electron image. The phase identification map in Figure 2(b) shows FCC iron (γ-austenite) in red, BCC iron (α-martensite) in blue, and HCP iron (ε-martensite) in yellow with grain boundaries and phase boundaries being distinguished by black lines. The EBSD phase identification is in good agreement with the phases and associated lattice parameters determined by XRD analysis as shown by the close match between the Kikuchi band pattern and the simulated HCP iron overlay shown in Figure 2(c) for point A in Figure 2(b). Presence of α-martensite is found both within areas of ε-martensite and of γ-austenite. Orientation with respect to the observed plane (Z axis) is shown in Figure 3 and reveals the observed area features a single austenite grain uniformly oriented with <111> very near the Z axis. Two orientations of ε-martensite are present. The first has a {0001}ε basal plane lying very near the observation plane resulting from sectioning parallel to the ε-martensite band thickness. The other orientation corresponds to an ε-martensite band sectioned on edge as shown in the right of Figure 3. Both instances of ε-martensite bands exhibit α-martensite in their interiors. The α-martensite lying in the ε- band oriented near the basal plane exhibits near-parallelism of {110}α' with the observation plane. Such planar parallelism and the subsequent orientation relationship (OR) are depicted by the colored phase boundaries in Figure 3. The Shoji-Nishyama (S-N) OR of $\{111\}\gamma \parallel \{0001\}\varepsilon, 110>\gamma \parallel <\bar{1}2\bar{1}0>\varepsilon$ denoted by a black phase boundary is present along every γ/ε interface [17]. Blue phase

boundaries distinguish a planar parallelism of {0001}ε || {110}α' which is present for every instance of α-martensite lying within an ε- band. All α-martensite lying within austenite exhibits a Kurdjumov-Sachs (K-S) OR of {111}γ || {110}α', <110>γ || <111>α' as denoted by white phase boundaries [18].

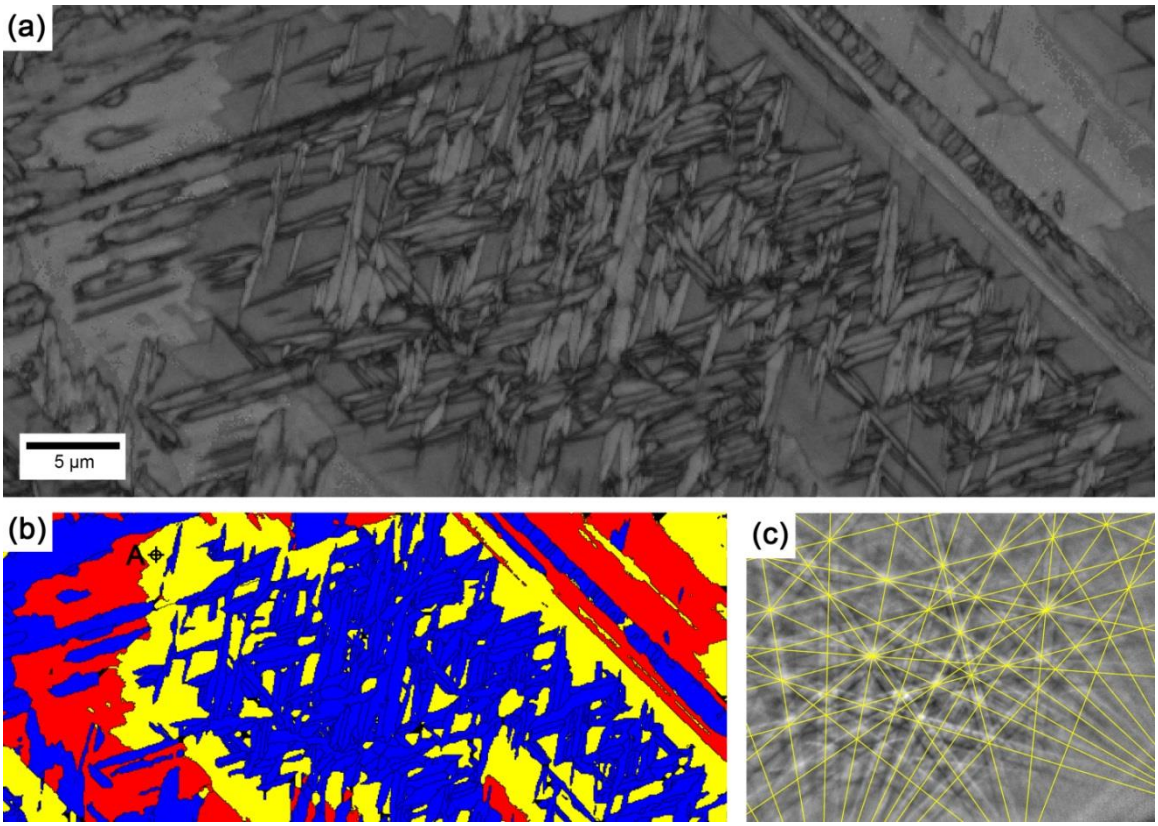

Figure 2. EBSD grain boundary and phase analysis of as-cast Fe-0.08C-15.1Mn-1.95Si-1.4Al-0.017N. (a) band contrast image and (b) phase identification where red is γ-austenite, blue is α-martensite, yellow is ε-martensite, and black lines are grain or phase boundaries. Kikuchi band pattern (c) from Point A in (b) matches well with the overlaid HCP simulation.

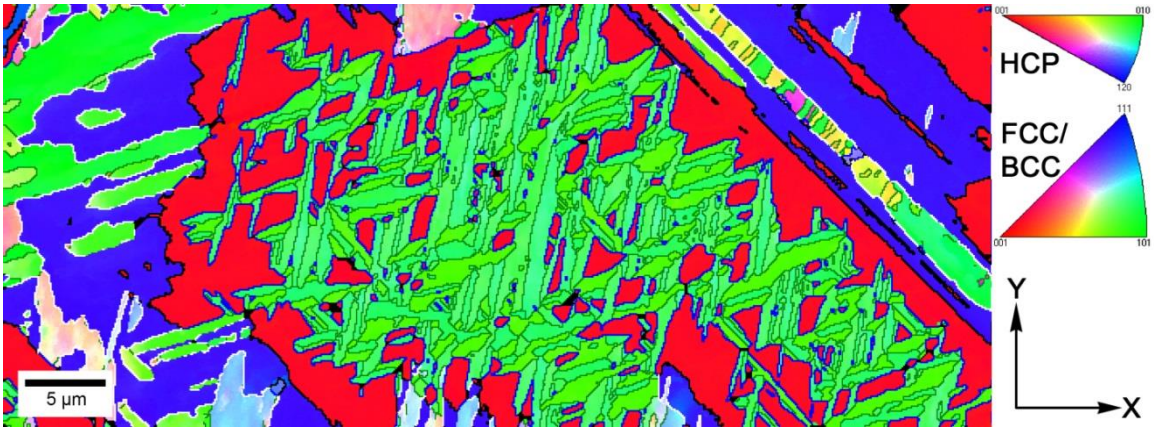

Figure 3. Orientation of the cubic and hexagonal phases with respect to the specimen normal (Z axis) in as-cast Fe-0.08C-15.1Mn-1.95Si-1.4Al-0.017N. Black boundaries denote {111}γ || {0001}ε, <110>γ || <$\bar{1}2\bar{1}0$>ε, white boundaries denote {111}γ || {110}α', <110>γ || <111>α', and blue boundaries denote {0001}ε || {110}α'.

Orientation of the α-martensite with respect to the X axis in the observed plane is shown in Figure 4 and reveals six distinct variants of α-martensite lying within the sectioned ε- band. The boundaries between variants correspond mostly to 60°<111> Σ3 boundaries (white lines) and 50°<110> Σ11 boundaries (black lines); however, misorientation angle/axis pairs of 10°<110> (green lines) and 60°<110> (yellow lines) were also present in some cases. The long direction of the α-martensite plate-like laths is <$1\bar{1}1$>α' and was parallel to <$\bar{1}2\bar{1}0$>ε to within 1° in the bulk and along α'/ε boundaries; however, instances of up to 7° deviation of <$1\bar{1}1$>α' from <$\bar{1}2\bar{1}0$>ε in the bulk were detected.

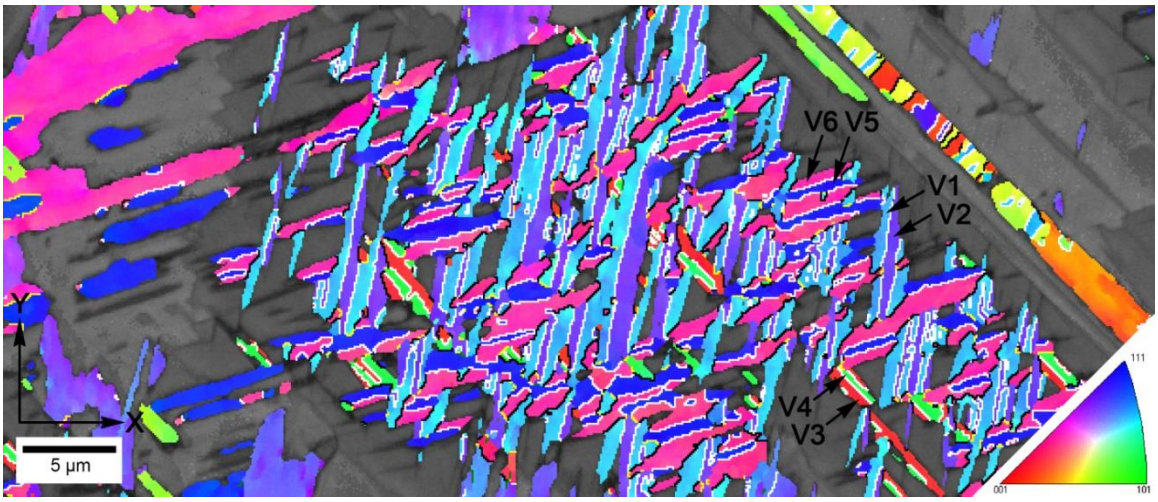

Figure 4. Orientation of α-martensite in as-cast Fe-0.08C-15.1Mn-1.95Si-1.4Al-0.017N shows six unique variants within an ε- band. Misorientation angle/axis pairs are as follows: 60°<111> Σ3 (white), 50°<110> Σ11 (black), 10°<110> Σ1 (green), and 60°<110> (yellow).

4. DISCUSSION

Previous studies on lath martensite nucleated from austenite have reported on the twenty-four α-martensite variants possible for the observed K-S OR and the calculated axis/angle misorientation between neighboring variants [19,20]. A similar approach was taken here to describe the variant OR and misorientations for α-martensite nucleated from ε-martensite as shown in Table 1 where a close packed directional parallelism of $<1\bar{1}1>\alpha'$ || $<\bar{1}2\bar{1}0>\varepsilon$ is assumed. Because ε- martensite is treated as the parent phase, only six unique α-martensite variants exist; however, if the Shoji-Nishiyama OR is considered, twenty-four variants of α-martensite become unique with respect to γ-austenite given the growth of four distinct ε- bands with the close packed planar parallelism $\{111\}\gamma$ || $\{0001\}\varepsilon$. Figure 5 depicts the six possible variants for a given parallelism $(0001)\varepsilon$ || $(110)\alpha$'. When plotted on the $(110)\alpha$' pole figure for the α-martensite in the widely sectioned ε- band in Figure 5, the calculated variant relations from Table 1 correlate well

with the observed variants as shown in Figure 6. Applying the corresponding variant numbers to the α-martensite laths in Figure 5 reveals that the six variants consist of three variant pairs, V1-V2, V3-V4, and V5-V6, which are twin related via 60°<111> and have a {112} twin plane. Further investigation of the $<1\bar{1}1>\alpha' \parallel <\bar{1}2\bar{1}0>\varepsilon$ parallelism is depicted in Figure 7 where the overlaid $<\bar{1}2\bar{1}0>\varepsilon$ directions correspond well to the $<1\bar{1}1>\alpha'$ body diagonals with deviation being less than 7°. It is also evident that the second body diagonal of any given variant deviates from the corresponding $<\bar{1}2\bar{1}0>\varepsilon$ by approximately 10.5° which can be shown to be the expected rotation for the lattice parameters calculated from XRD analysis of $a_{\alpha\text{-martensite}}$= 2.88Å and $a_{\varepsilon\text{-martensite}}$= 2.54Å.

Table 1. Six variants of α-martensite nucleated from ε-martensite and the misorientation between them.

Variant No	Plane Parallel	Direction Parallel [uvw]ε || [uvw]α'	Rotation from Variant 1	
			Angle (°)	Axis
V1	(0001)ε || (110)α'	$[\bar{1}2\bar{1}0] \parallel [1\bar{1}\bar{1}]$	---	---
V2		$[\bar{1}2\bar{1}0] \parallel [1\bar{1}1]$	60.0	$[\bar{1}11]\alpha'$
V3		$[2\bar{1}\bar{1}0] \parallel [1\bar{1}\bar{1}]$	60.0	$[110]\alpha'$
V4		$[2\bar{1}\bar{1}0] \parallel [1\bar{1}1]$	10.5	$[\bar{1}\bar{1}0]\alpha'$
V5		$[\bar{1}\bar{1}20] \parallel [1\bar{1}\bar{1}]$	60.0	$[\bar{1}\bar{1}0]\alpha'$
V6		$[\bar{1}\bar{1}20] \parallel [1\bar{1}1]$	49.5	$[110]\alpha'$

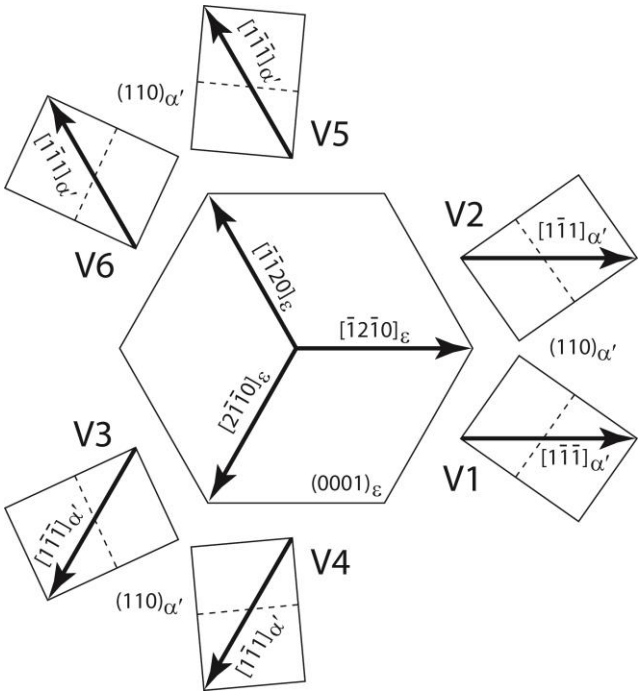

Figure 5. Six possible α-martensite variants nucleated from ε-martensite for a given plane parallelism (0001)ε || (110)α'.

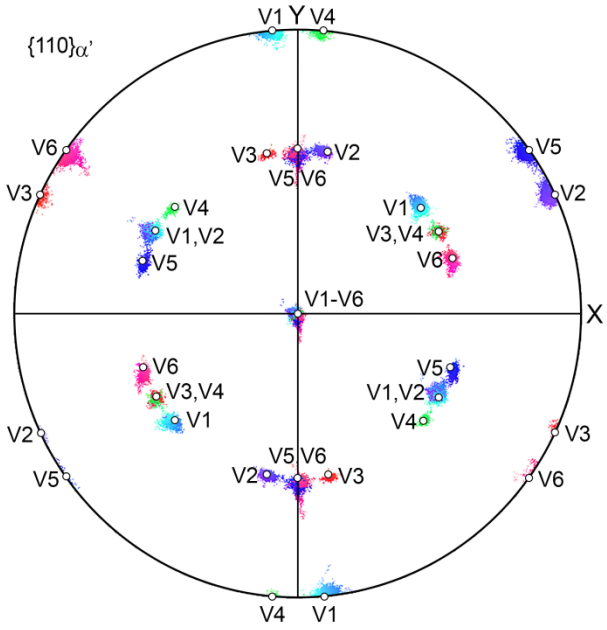

Figure 6. Calculated and experimental α-martensite variants nucleated from ε-martensite on a {110}α' pole figure.

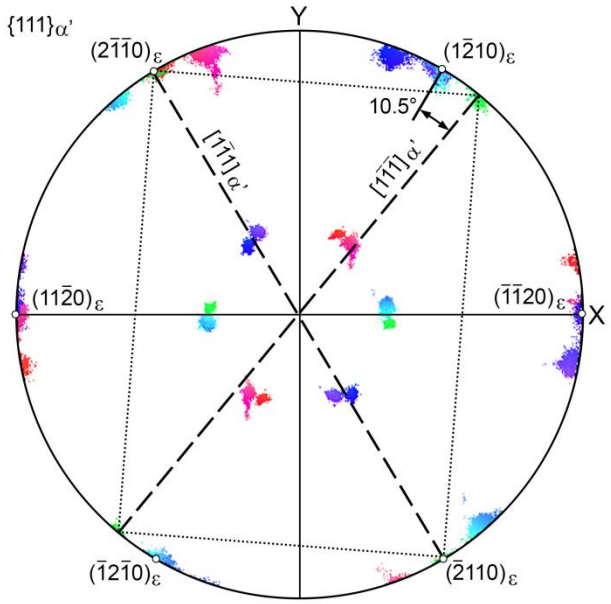

Figure 7. Calculated and experimental parallel relationship between α-martensite body diagonals <1$\bar{1}$1>α' and <$\bar{1}$2$\bar{1}$0>ε. Variant 4 is depicted schematically for reference.

Twin related α-martensite pairs nucleated athermally from ε-martensite have been reported by Kelly [21] in a Fe-12.2Mn-10.5Cr-4.1Ni-0.03C steel which was quenched to 77K (-196°C). Single-surface trace analysis showed that the habit plane of the α-martensite was {$\bar{1}\bar{1}$2}γ perpendicular to the {111}γ plane of the ε- band formation. Kelly only observed one variant pair in a given ε- band due to the limited field of view of transmission electron microscopy but theorized that three variant pairs (six variants total) were possible for any given ε- band. Shimizu and Tanaka [22] confirmed this theory by observing all six variants of the orientation relationship in a Fe-12Mn-0.48C alloy quenched to 218K (-55°C). Two-surface trace analyses revealed that the habit plane normals of the α-martensite made three pairs of two centered about the three {11$\bar{2}$}γ poles but the normals of each pair deviated from their respective pole in opposite directions by about 7°. Shimizu and Tanaka [22] showed that the junction plane between

the two variants of a pair was equivalent to their mirror plane described as $\{2\bar{1}1\}\alpha'$, or perhaps more appropriately $\{1\bar{1}00\}\varepsilon$. Kelly [21] has shown that an invariant shear system of $\{111\}\gamma<\bar{1}2\bar{1}>\gamma$ more appropriately describes the occurrence of $\{\bar{1}\bar{1}2\}\gamma$ type α-martensite habit planes rather than the typical $\{110\}\gamma<1\bar{1}0>\gamma$ system reported for lath martensite which has habit planes near $\{225\}\gamma$ and forms following a K-S OR [19,20]. This theory can be applied here to describe $\{0001\}\varepsilon<1\bar{1}00>\varepsilon$ as the active invariant shear system for the ε→α' athermal transformation in Fe-0.08C-1.95Si-15.1Mn-1.4Al-0.017N steel. EBSD analysis of a Fe-15.2Cr-5.7Ni-5.5Mn-0.06C alloy by Weidner et al. [4] revealed twin related (Σ3) boundaries and 50°<110> (Σ11) boundaries between α-martensite variants present in ε- bands after cyclic deformation. Such findings suggest a six variant, $\{0001\}\varepsilon<1\bar{1}00>\varepsilon$ invariant shear nucleation mechanism likely occurs for strain-induced martensitic transformations as well as athermal transformations.

In both the study by Kelly [21] and by Shimizu and Tanaka [22], no α-martensite was found nucleated from γ-austenite and only the γ→ε→α' transformation was reported. Here, the athermal γ→ε→α' transformation is shown in a Fe-0.08C-1.95Si-15.1Mn-1.4Al-0.017N alloy with low calculated stacking fault energy (-2.1 mJ/m^2) and subsequent M_S^{ε} temperature of 311K (38°C) and $M_S^{\alpha'}$ temperature of 347K (74°C) as determined via a relation by De Cooman and Spear [23]. Unlike previous studies, this alloy also showed areas of γ→α' athermal martensitic transformation. These areas exhibited typical K-S OR expected for lath martensite nucleated from γ-austenite [19,20] which is likely a result of $M_S^{\alpha'}$ being greater M_S^{ε} in this alloy and the γ→α' reaction preceding ε-martensite formation. The K-S OR present in this alloy is consistent with other observations of γ→α'K-S OR in which the invariant shear system has been shown

to be $\{110\}\gamma<1\bar{1}0>\gamma$ [19]. In conjunction with the proposed theory by Kelly [21], it is apparent that two unique and independent martensitic transformations may occur in this alloy: (1) athermal $\gamma\rightarrow\alpha'$ via a typical $\{110\}\gamma<1\bar{1}0>\gamma$ invariant shear system which has been shown [19] to form twenty four variants expected for the K-S OR and (2) athermal $\gamma\rightarrow\varepsilon\rightarrow\alpha'$ with the later transformation forming via a $\{0001\}\varepsilon<1\bar{1}00>\varepsilon$ invariant shear system forming six α-martensite variants.

5. CONCLUSIONS

Electron backscatter diffraction analysis has revealed the presence of athermal ε- and α- martensite in the as-cast structure of a Fe-0.08C-1.95Si-15.1Mn-1.4Al-0.017N alloy. The Shoji-Nishiyama orientation relationship was observed between γ-austenite and ε-martensite while α-martensite nucleated from γ-austenite exhibited a Kurdjumov-Sachs orientation relationship with its parent phase. Six crystallographic variants of α-martensite consisting of three twin-related variant pairs were observed in ε- bands. A planar parallelism of $\{0001\}\varepsilon \parallel \{110\}\alpha'$ and a directional relation of $<1\bar{1}1>\alpha'$ lying within 1° of $<\bar{1}2\bar{1}0>\varepsilon$ existed for these variants. The alloy exhibited two athermal martensitic transformation described by $\gamma\rightarrow\alpha'$ and $\gamma\rightarrow\varepsilon\rightarrow\alpha'$ where a $\{110\}\gamma<1\bar{1}0>\gamma$ invariant shear system is proposed for the former transformation and a $\{0001\}\varepsilon<1\bar{1}00>\varepsilon$ invariant shear system is proposed for the latter transformation.

ACKNOWLEDGEMENTS

This work was supported by the Peaslee Steel Manufacturing Research Center (PSMRC). The authors gratefully acknowledge Rod Grozandich of Spokane Industries, Inc. for casting the alloy. The FEI Helios NanoLab dual beam FIB was obtained with a

Major Research Instrumentation grant from the National Science Foundation under contract DMR-0723128. The authors also acknowledge the support of the Materials Research Center and in particular Dr. Clarissa Wisner and Dr. Jessica TerBush for guidance and training in using the FIB.

REFERENCES

[1] B. Cina: *Acta Metall.*, 1958, vol. 6, pp. 748-62.

[2] I.V. Kireeva and Y.I Chumlyakov: *Phys. Met. Metallogr.*, 2006, vol. 101, pp. 186-203.

[3] H. Fujita and S. Ueda: *Acta Metall.*, 1972, vol. 20, pp. 759-67.

[4] A. Weidner, A. Glage, and H. Bierman: *Procedia Eng.*, 2010, vol. 2, pp. 1961-71.

[5] C.X. Huang, G. Yang, Y.L Gao, S.D. Wu, and S.X. Li: *J. Mater. Res.*, 2007, vol. 22 (3), pp. 724-729.

[6] J. Talonen and H. Hänninen: *Acta Mater.*, 2007, vol. 55, pp. 6108-18.

[7] G.B. Olson and M. Cohen: *J. Less-Common Met.*, 1972, vol. 28, pp. 107-18.

[8] B. Jiang, X. Qi, S. Yang, W. Zhou, and T.Y. Hsu: *Acta Mater.*, 1998, vol. 46 (2), pp. 501–10.

[9] O. Grässel, G. Frommeyer, C. Derder, and H. Hofmann: *J.Phys. IV France*, 1997, vol. 7, pp. C5-383-88.

[10] G. Olson and M. Cohen: *Metall. Mater. Trans. A*, 1976, vol. 7, pp. 1897-1904.

[11] M. Koyama, T. Sawaguchi, T. Lee, C.S. Lee, and K. Tsuzaki: *Mater. Sci. Eng. A*, 2011, vol. 528, pp. 7310-16.

[12] J.C. Kim, D.W. Han, S.H. Baik, Y.K. Lee: *Mater. Sci. Eng., A*, 2004, vol. 378, pp. 323-327.

[13] M.C. McGrath, D.C. Van Aken, N.I. Medvedeva, and J.E. Medvedeva: *Metall. Mater. Trans. A*, 2013, vol. 44A, pp. 4634-43.

[14] D.K. Matlock and J.G. Speer: Proceedings of the 3rd Int. Conf. on Structural Steels, ed. By H.C. Lee, *The Korean Institute of Metals and Materials*, Seoul, Korea, 2006, pp 774-781.

[15] A.K. De, D.C. Murdock, M.C. Mataya, J.G. Speer, and D.K. Matlock: *Scr. Mater.*, 2004, vol. 50, pp. 1445-49.

[16] S. Martin, C. Ullrich, D. Šimek, U. Martin, and D. Rafaja, *J. Appl. Crystallogr.*, 2011, vol. 44, pp. 779-787.

[17] Z. Nishyama: Martensitic Transformation, Academic Press, Inc., New York, NY, 1978, p. 49.

[18] G. Kurdjumov and G. Sachs: *Z. Phys.*, 1930, vol. 64, pp. 325-343.

[19] S. Morito, H. Tanaka, R. Konishi, T. Furuhara, and T. Maki: *Acta Mater.*, 2003, vol. 51, pp. 1789-1799.

[20] H. Kitahara, R. Ueji, N. Tsuji, and Y. Minamino: *Acta Mater.*, 2006, vol. 54, pp. 1279-1288.

[21] P.M. Kelly: *Acta Metall.*, 1965, vol. 13, pp. 635-46.

[22] K. Shimizu and Y. Tanaka: *Trans. Jpn. Inst. Met.*, 1978, vol. 19, pp. 685-693.

[23] B.C. De Cooman and J.G. Speer: Fundamentals of Steel Product Physical Metallurgy, 1st ed., ASM International, Novelty, OH, 2011, p. 173.

SECTION

2. FUTURE ALLOY DESIGN

2.1. INTRODUCTION

The successful completion of a self-consistent thermodynamic model has produced a viable tool for the prediction of phase development in FeMnAlSiC TRIP steels. The model will be used to here to determine the effect of Mn, Si and Al additions on thermodynamic driving forces for the $\gamma \rightarrow \varepsilon$, $\gamma \rightarrow \alpha'$ and $\varepsilon \rightarrow \alpha'$ transformations in an attempt to determine optimized compositions.

2.2. PROCEDURE

Alloy optimization involved the active varying of Mn, Si and Al between the values listed in Table 2.1. Carbon and nitrogen levels were fixed at 0.07 wt% and 0.017 wt%, respectively, and Fe was allowed to vary as needed to fulfill the normalization requirements for ternary plots. It is important to note that in this investigation nitrogen is treated only as a weight percent placeholder. While the importance of nitrogen content on ε-martensite formation is realized, the effect of nitrogen on driving force was not modeled by this simulation. As such, a nitrogen value equal to that of McGrath's et al. [6] composition was assumed to be optimal.

Table 2.1. Alloy ranges (weight %) investigated for optimization.

	Active Variables			Consequent Variable	Fixed Values	
	Mn	Si	Al	Fe	C	N
Max	20.0	4.0	2.5	73.413	0.07	0.017
Min	10.0	1.0	0.5	88.413		

Driving forces for the γ→ε, γ→α' and ε→α' transformations were plotted using OriginLab9 in a ternary fashion where the axes depict Si, Mn, and Fe+C+N; however, it is important to note that only Fe content is changing for the Fe+C+N axis. Separate plots were generated for each Al content from 0.5% to 2.5% in increments of 0.5%. Iso-driving force lines (dotted lines) have been added corresponding to the calculated driving forces for the alloys listed in Table 2.2 in an effort to relate future alloy development to examined microstructures and tensile behaviors reported in the literature.

Similar optimization plots were made for the M_S^{ε}, $M_S^{\alpha'}$ and ΔM_S ($M_S^{\varepsilon} - M_S^{\alpha'}$) temperatures. The M_S^{ε} temperature was calculated for a nucleating defect size of $n = 6$ and the $M_S^{\alpha'}$ temperature was calculated using Eq. 1.2. Isothermal lines (dotted lines) have been added corresponding to calculated martensite start temperatures for the alloys listed in Table 2.2.

Table 2.2. FeMnAlSiC alloys used for comparison in optimization analysis.

	Composition (wt pct)				
Alloy	Mn	Si	Al	C	N
(A) McGrath et al.[6]	15.3	2.85	2.4	0.07	0.017
(B) Van Aken et al.[7]	14.2	1.85	2.38	0.06	0.019
(C) Pisarik et al.[30]	15.1	1.95	1.4	0.08	0.017
(D) Paper I	13.9	2.07	2.01	0.09	0.012
(E) Pisarik et al.[30]	14.3	2.97	0.89	0.16	0.022
(F) Frommeyer et al.[39]	15.8	3.00	2.9	0.02	---
(G) Yang et al.[31]	21.5	0.19	---	0.24	---

2.3. RESULTS

The effect of Mn, Si and Al on calculated transformation driving forces is shown in Figure 2.1. The driving force for ε-martensite formation becomes more negative for lower alloying levels and reaches a local minimum at a composition of Fe-13Mn-1.0Si-0.5Al-0.07C-0.017N (see Figure 2.1(a)). Increasing aluminum content has the most deleterious effect (per weight %) on the driving force of ε-martensite formation from austenite. The reaction to form ε-martensite is no longer spontaneous for compositions that contain Al contents greater than 2.5%. Richer Al contents also marginally decrease the driving force for α-martensite formation from austenite as shown in Figure 2.1(b). Despite aluminum's effect on increasing the $M_S^{\alpha'}$ temperature and stabilizing ferrite, the displacement of Fe, and its inherent driving force, with Al marginally decreases the magnitude of $\Delta G^{\gamma\rightarrow\alpha'}$. Manganese levels approaching 10% increase favorability of the γ→α' transformation and the effect of Si is minimal. The driving forces for the ε→α' transformation in Figure 2.1(c) are similar in nature to the γ→α' transformation in Figure 2.1(b) because the magnitudes of $\Delta G^{\gamma\rightarrow\alpha'}$ are significantly greater than the magnitudes of $\Delta G^{\gamma\rightarrow\varepsilon}$. However, of notable difference is the effect of increased Al content which favors the ε→α' transformation as opposed to suppressing γ→α' transformation.

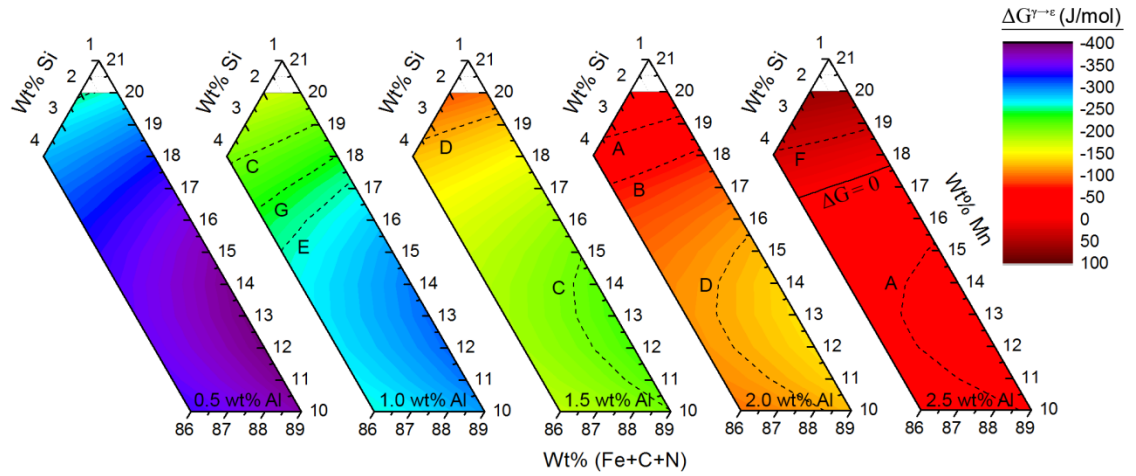

(a)

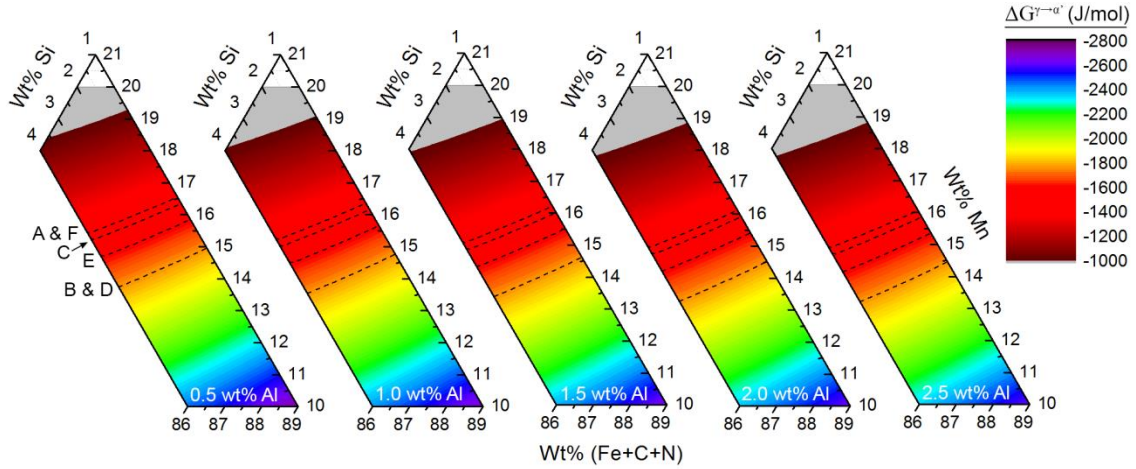

(b)

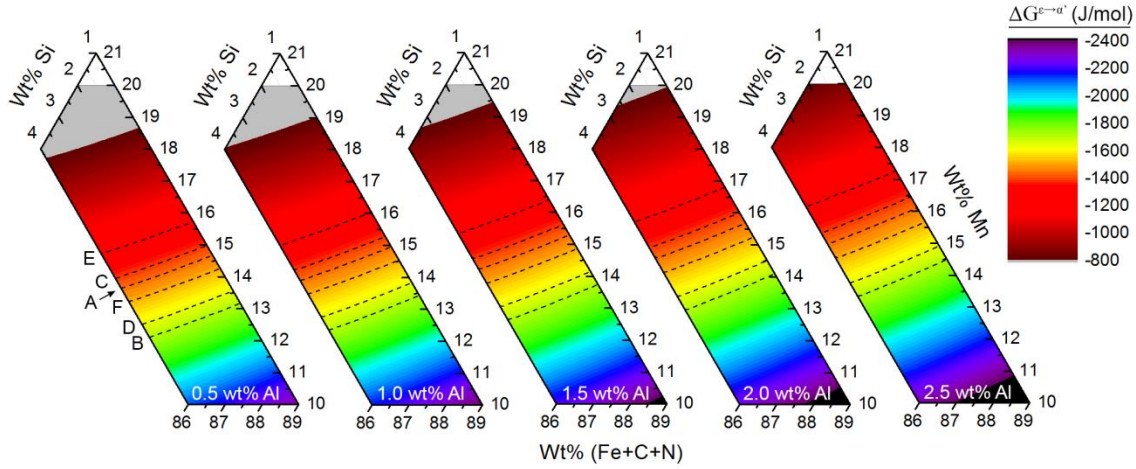

(c)

Figure 2.1. Thermodynamic driving forces for the (a) γ→ε, (b) γ→α' and (c) ε→α' transformations in FeMnAlSiC alloys. Dotted lines are iso-driving force lines and correspond to the alloy letter designations in Table 2.2. Values of 0.07wt% C and 0.017 wt% N were held constant.

The M_S^{ε} temperature has been calculated via the approach outlined in Paper I and as such is directly related to $\Delta G^{\gamma \rightarrow \varepsilon}$. Thus, the dependence of M_S^{ε} temperature on composition shown in Figure 2.2(a) is similar to that seen for $\Delta G^{\gamma \rightarrow \varepsilon}$ in Figure 2.1(a). The highest calculated M_S^{ε} temperature (111°C) is related to a lean composition of Fe-13Mn-1.0Si-0.5Al-0.07C-0.017N. Richer compositions, specifically aluminum contents between 1.5 and 2.0 wt%, suppress M_S^{ε} below room temperature. In contrast, Figure 2.2(b) reveals that increasing aluminum content increases the $M_S^{\alpha'}$ temperature by a rate of 30°C/wt%. Additionally, athermal α-martensite nucleated via the $\gamma \rightarrow \alpha'$ transformation is favorable upon quenching to room temperature in alloys with less than 16 wt% Mn regardless of Al or Si content. Compositions which are lean in Al (0.5 wt%) and have greater than 13.5 wt% Mn can form athermal ε-martensite upon quenching from austenite before the athermal α-martensite transformation begins. Increasing Al contents to 1 or 1.5 wt% augments this phenomenon to a higher required Mn level of 15 and 17 wt%, respectively. Silicon has a negligible effect on the difference between M_S^{ε} and $M_S^{\alpha'}$ temperature.

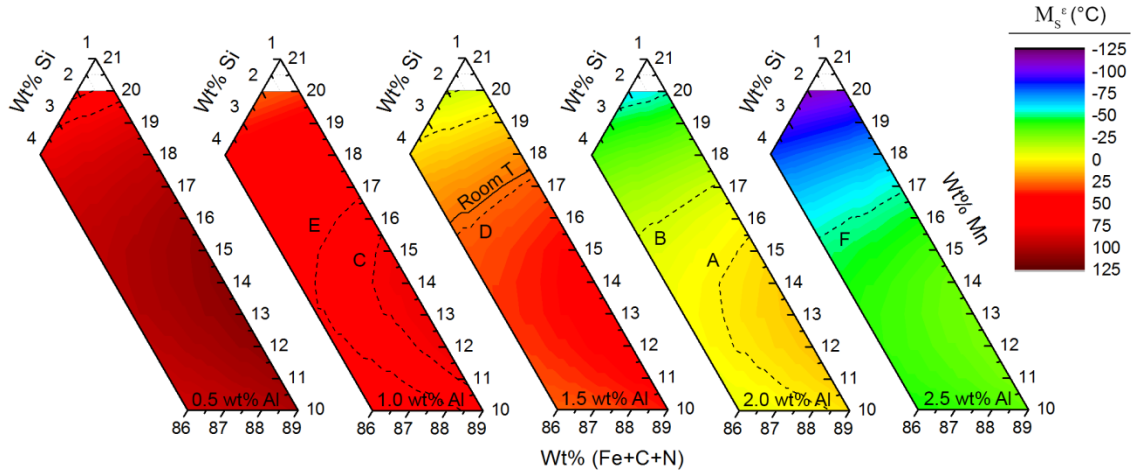

(a)

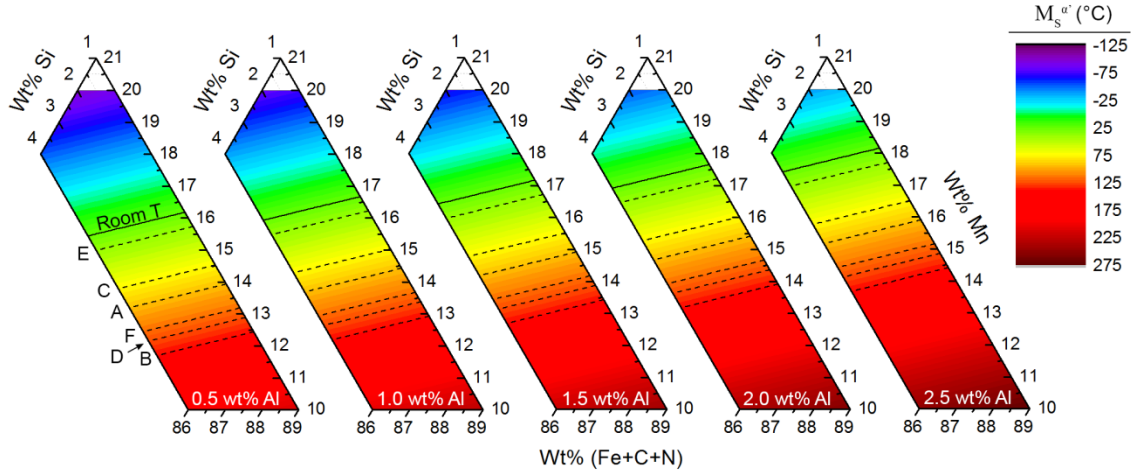

(b)

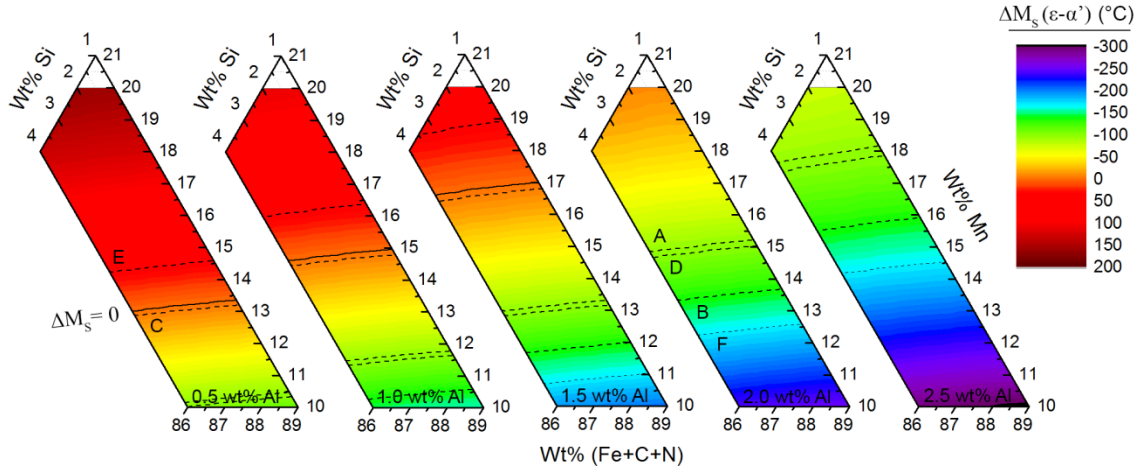

(c)

Figure 2.2. The effect of composition on (a) M_S^{ε} (n = 6), (b) $M_S^{\alpha'}$ and (c) $M_S^{\varepsilon} - M_S^{\alpha'}$ temperatures in FeMnAlSiC alloys. Dotted lines are iso-thermal lines and correspond to the alloy letter designations in Table 2.2. Values of 0.07wt% C and 0.017 wt% N were held constant.

2.4. DISCUSSION

The promotion of the γ→ε transformation is strongly influenced by alloying content as observed in Figure 2.1. Mn has a complex effect where a local minimum in $\Delta G^{\gamma\rightarrow\varepsilon}$ develops around 13 wt% Mn regardless of other alloying. This effect, determined thermodynamically, is in excellent agreement with the first-principles calculations performed by Medvedeva et al. [18] which suggest a minimum in ISFE (and subsequently $\Delta G^{\gamma\rightarrow\varepsilon}$ via Eq. 1.1) is present at 12.5 at% Mn. It can be shown that 13 wt% Mn equates to 12.3-12.9 at% when present in alloys with 1-4 wt% Si and 0.5-2.5 wt% Al as investigated here. Likewise, the decrease in γ→ε thermodynamic driving force with increased Al content also corroborates the findings of Medvedeva et al. [18] that Al additions decrease ISFE. In a similar manner, Si additions also decrease γ→ε thermodynamic driving force and have been shown by first-principles calculation to decrease ISFE akin to Al [30]. The agreement between both calculation techniques suggests both models can be used in conjunction in future alloy design which is a necessity given thermodynamic predictions cannot address the effect of alloying additions on USFE. Pisarik et al. [30] have determined Si to lower the USFE in a similar manner to Al and as such Si should promote the formation of Shockley partial dislocations responsible for ε-martensite nucleation. The thermodynamic calculations performed here suggest Si decreases the γ→ε driving force by 15 J/mol/wt%Si on average compared to the average decrease imposed by Al of 160 J/mol/wt%Al. Thus, the substitution of Si for Al, for example in an alloy with 2.5 wt% Si and 0.5 wt% Al, is beneficial in maintaining low USFE and ease of ε-martensite nucleation while also preserving ε-martensite stability relative to austenite ($\Delta G^{\gamma\rightarrow\varepsilon}<0$).

It is important to note that the stabilization of ε-martensite relative to austenite is only advantageous so long as there exists ample driving force for the ε→α' transformation to avoid premature fracture associated with over-stabilized ε-martensite as observed in Alloy E [30]. The suggested lowering of aluminum content to promote the γ→ε transformation will also decrease the ε→α' driving force as shown by Figure 2.1(c). However, second stage driving forces can be restored by the lowering of Mn at an average rate of approximately (-)180 J/mol/wt%Mn near compositions of 15 wt% Mn. For the aforementioned 2.5 wt% Si and 0.5 wt% Al alloy, a Mn content less than 15.2 wt% increases the ε→α' driving force above the Alloy E isopleth while decreasing Mn to 12.7 wt% further promotes the transformation to an extent near Alloy B which exhibited complete transformation [7].

Of further consideration is martensite start temperature. The suggested low Al content of 0.5 wt% favors M_S^{ε} and suppresses $M_S^{\alpha'}$ such that ε-martensite should form prior to α-martensite upon quenching in alloys with Mn content greater than 13.4 wt%. As such, a future composition Fe-14Mn-2.5Si-0.5Al-0.07C-0.017N may be of interest and is listed as Alloy 1 in Table 2.3. In this alloy, ε-martensite has been stabilized relative to austenite to such a degree that calculated room temperature ISFE is negative. This value implies that the high temperature austenitic mictrostructure should exhibit near complete transformation to ε-martensite upon cooling to room temperature. The lack of retained austenite in Alloy E is believed to have led to the absence of Stage I (γ→ε) TRIP during tensile testing [30] and it is likely the near complete transformation in Alloy 1 would result in a similar behavior. However, a fully ε-martensitic structure has yet to be characterized under tensile behavior. With a stronger driving force for Stage II

(ε→α') TRIP than Alloy E, Alloy 1 may fully elongate to necking and thus exhibit significantly increased UTS through work hardening. Furthermore, recent intercritical annealing trials of FeMnAlSiC steels bearing 7 wt% Mn have produced partitioned austenite which transformed to ε-martensite upon quenching. As such, the characterization of a fully ε-martensitic steel may be of significant scientific interest in understanding tensile behavior of other alloy systems which exhibit local regions of ε-martensite. In a similar regard, Alloy 2 of composition Fe-10Mn-2.5Si-0.5Al-0.07C-0.017N may also be of interest. Here, Mn content has been decreased in an attempt to increase manufacturability of the alloy to address industrial concerns of Mn ladle additions and volatilization associated with high alloying requirements. Because of the complex effect of Mn on the γ→ε transformation, the driving force for Stage I TRIP remains relatively unchanged. However, the decreased austenite stability relative to α-martensite has significantly increased the driving force for Stage II TRIP to (-)2228 J/mol and has increased the $M_S^{\alpha'}$ temperature 82°C above the M_S^{ε} temperature. As such, the room temperature stable microstructure will likely exhibit an increased fraction of α-martensite relative to Alloy 1 but should serve to aid the evaluation of the lower Mn variants of FeMnAlSiC TRIP steels, which may only exhibit single stage behavior.

Table 2.3. Suggested FeMnAlSiC TRIP compositions for future investigation. Composition is in weight percent.

Alloy	$\Delta G^{\gamma\rightarrow\varepsilon}$ (J/mol)	$\Delta G^{\varepsilon\rightarrow\alpha'}$ (J/mol)	ISFE (mJ/m^2)	M_S^{ε} (°C)	$M_S^{\alpha'}$ (°C)
(1) Fe-14Mn-2.5Si-0.5Al-0.07C-0.017N	-364	-1460	-1.5	130	80
(2) Fe-10Mn-2.5Si-0.5Al-0.07C-0.017N	-358	-2228	-1.1	120	202
(3) Fe-14Mn-2.5Si-0.5Al-0.15C-0.017N	-329	-1320	0.6	116	46
(4) Fe-10Mn-2.5Si-0.5Al-0.15C-0.017N	-316	-2085	1.4	105	168
(5) Fe-14Mn-2.5Si-1.5Al-0.07C-0.017N	-200	-1561	8.2	65	110
(6) Fe-15Mn-2.5Si-1.3Al-0.07C-0.017N	-223	-1368	6.8	75	73
(7) Fe-11Mn-2.5Si-1.3Al-0.07C-0.017N	-233	-1717	6.2	79	195
(8) Fe-12Mn-2.5Si-1.3Al-0.15C-0.017N	-202	-1763	8.1	64	131

The primary objective of this investigation was the optimization of composition to obtain two-stage TRIP behavior. The stability of ε-martensite over austenite in Alloys 1 and 2 will likely suppress Stage I TRIP. As such, it was desirable to lessen the $\gamma\rightarrow\varepsilon$ driving force such that a moderate ISFE near 10 mJ/m^2 is developed which should retain room stable austenite upon quenching but still promote the $\gamma\rightarrow\varepsilon$ transformation upon deformation. One avenue for achieving this is the increase of carbon content which has proved to suppress both M_S temperatures (Figure 1.9) via the stabilization of austenite. Increasing C to 0.15 wt% in Alloys 1 and 2 produces Alloys 3 and 4 shown in Table 2.3 and effectively increases ISFE to 0.6 and 1.4 mJ/m^2, respectively. The marginal increase in ISFE has suppressed the M_S^{ε} temperature by approximately 15°C in both alloys which is likely not sufficient to greatly increase the amount of retained austenite. Of greater impact may be the 34°C decrease in $M_S^{\alpha'}$ temperature between Alloy 1 and 3 and between Alloy 2 and 4 that could lessen the fraction of α-martensite formed upon quenching in favor of TRIP capable phases, be they austenite or ε-martensite. Koistenen

and Marburger [40] have described the extent of conventional γ→α' martensitic transformation by relating the volume fraction of α-martensite, $V_{\alpha'}$, developed upon quenching to some temperature, T_q, via the expression:

$$1-V_{\alpha'} = \exp\left\{\beta\left(M_S - T_q\right)\right\} \quad \text{where } \beta \cong -0.011 \tag{2.1}$$

While this relation is not directly applicable to the triplex microstructures examined here, which also nucleate α-martensite via the ε→α' transformation, it can be used to indicate the general degree of austenite retention. Using Eq. 2.1, a retained austenite volume percent of 14.3 is predicted for Alloy 2 (0.07 wt% C) and 20.7 is predicted for Alloy 4 (0.15 wt% C). As such, varying C may not produce a significant change in retained austenite fraction.

Altering Mn or Al levels has stronger influence on $\Delta G^{\gamma\rightarrow\varepsilon}$ and ISFE than C. The γ→ε transformation driving force is mitigated as Mn is deviated in either direction from the 13 wt% local maximum. Increasing Mn concentration above 15 wt% is not advantageous as this will incur significant increases in alloying cost and limit manufacturability. Decreasing Mn concentration near 10 wt% significantly decreases austenite stability relative to α-martensite as shown in Figure 2.1(b) and increases $M_S^{\alpha'}$ temperature above 200°C regardless of other alloying additions as shown in Figure 2.2(b). In this regard, a predominately α-martensitic structure would be expected to form upon quenching and would limit the amount of TRIP capable phases and material ductility. As such, the variation of Mn in an effort to control austenite stability is not suggested. Limiting Al addition to less than 1.5 wt% will maintain a γ→ε driving force greater than (-)200 J/mol in a 15 wt% Mn alloy while also preserving a M_S^{ε} temperature

greater than room temperature. However, it should be noted that M_S^{ε} temperature can be influenced by process history and as such higher aluminum additions of 2 wt% can still produce significant ε-martensite fractions (e.g. 60 and 29 vol% in hot rolled Alloys A and B, respectively [2,4]). Higher aluminum concentrations of 2 wt% or greater also induce greater α-martensite stability and significantly increase $M_S^{\alpha'}$ temperatures above 100°C. As such, despite aluminum's effect of destabilizing ε-martensite in an effort to retain austenite, the austenite will instead have a greater preference for α-martensite formation and ultimately the degree of retained austenite in the quench structure may remain unchanged. Regardless, Al may be the most influential alloying constituent that can be controlled to tailor microstructure phase fractions. For the optimal promotion of two-stage TRIP behavior, an intermediate Al content near 1.5 wt% is recommended.

Alloy 5, with a composition of Fe-14Mn-2.5Si-1.5Al-0.07C-0.017N, has a moderate $\gamma \rightarrow \varepsilon$ driving force of (-)200 J/mol and an ISFE of 8.2 mJ/m^2 which should aid the retention of austenite. The limiting of Al content to 1.5 wt% results in a calculated $M_S^{\alpha'}$ temperature of 110°C which should ensure incomplete transformation of austenite (40 vol% retained austenite predicted by Eq. 2.1) thus providing a balanced triplex microstructure that may exhibit complete two-stage TRIP behavior due to the strong driving force for the $\varepsilon \rightarrow \alpha'$ transformation. The stability of α-martensite relative to ε-martensite is greater for Alloy 5 ($\Delta G^{\varepsilon \rightarrow \alpha'}$ = -1561 J/mol) than that of Alloy E ($\Delta G^{\varepsilon \rightarrow \alpha'}$ = -1260 J/mol) which exhibited premature failure from over-stabilized ε-martensite. Lowering of the $M_S^{\alpha'}$ temperature, and subsequent reduction of the fraction of α-martensite in the quenched microstructure, can be obtained by increasing the Mn content to 15 wt% and decreasing Al to 1.3 wt% as outlined in Alloy 6. This composition change

also decreases ISFE and thus more ε-martensite formation and less retained austenite may be expected compared to Alloy 5. As such, this alteration should only be made if Alloy 5 proves to produce an excess of α-martensite such that TRIP ductility is limited.

Of final concern may be the reduction of Mn content in an effort to aid manufacturability. Alloys 2 and 4 addressed this concern by reducing Mn to 10 wt% but will likely lack sufficient retained austenite to exhibit two-stage TRIP behavior. Alloy 7 alleviates this problem by combing 11 wt% Mn with 1.3 wt% Al where the Al acts to destabilize ε-martensite resulting in a calculated ISFE of 6.2 mJ/m^2. The reduction of Mn has subsequently increased α-martensite stability ($\Delta G^{\gamma\rightarrow\alpha'} = -2332$ J/mol) and $M_S^{\alpha'}$ temperature to 195°C and as such a significant fraction of austenite is likely to transform to α-martensite upon quenching (85 vol% transformed predicted by Eq. 2.1). These effects can be mitigated by increasing Mn content to 12 wt% and C content to 0.15 wt% as shown in Alloy 8. The calculated $M_S^{\alpha'}$ temperature is decreased 64°C and as such the presence of 31 vol% retained austenite upon quenching to room temperature it predicted by Eq. 2.1. Further, the increased C content has increased the calculated ISFE to 8.1 mJ/m^2 thereby decreasing the extent of athermal γ→ε transformation in comparison to Alloy 7 while still maintaining sufficient driving force for Stage I TRIP. As such, Alloy 8 is recommended if lower Mn concentrations are preferred.

2.5. CONCLUSIONS

The thermodynamic model derived in Paper I has been used to calculate driving forces and martensite start temperatures for the γ→ε→α' transformation in FeMnAlSiC steels with compositions between 10-20 wt% Mn, 1-4 wt% Si and 0.5-2.5 wt% Al in an attempt to determine optimal alloy combinations which may be of further interest. The

model's predicted influence of Mn, Si and Al on SFE and the γ→ε transformation are in excellent agreement with ab-initio calculations. Aluminum was found to have the most significant influence on γ→ε driving force. Alloys with composition low Al contents such as Fe-14Mn-2.5Si-0.5Al-0.07C-0.017N exhibit calculated ISFE less than zero and as such are likely to fully transform upon quenching and lack sufficient amounts of retained austenite to produce Stage I TRIP (γ→ε). These alloy combinations are of scientific interest in determining tensile properties of the yet uncharacterized steels that solely exhibit Stage II TRIP (ε→α') behavior. To induce austenite stability, higher Al compositions such as Fe-14Mn-2.5Si-1.5Al-0.07C-0.017N adequately balance ε- and α-martensite start temperatures such that some retained austenite is expected upon quenching to room temperature. The Fe-14Mn-2.5Si-1.5Al-0.07C-0.017N alloy exhibits calculated transformation driving forces of $\Delta G^{\gamma\rightarrow\varepsilon}$ = -200 J/mol and $\Delta G^{\varepsilon\rightarrow\alpha'}$ = -1561 J/mol which are estimated as sufficient to ensure full two-stage TRIP behavior and avoid premature fracture from phase over-stabilization. Also suggested here is the examination of an alloy with composition Fe-12Mn-2.5Si-1.3Al-0.15C-0.017N which exhibits similar phase stability and driving force of the Fe-14Mn-2.5Si-1.5Al-0.07C-0.017N alloy but substitutes an increased carbon content such that manganese concentration can be lowered to 12 wt% in an attempt to increase alloy manufacturability via conventional continuous steelmaking operations.

3. CONCLUSIONS

A review of thermodynamic models for the prediction of driving force for the γ→ε, γ→α', and subsequent ε→α' martensitic transformations for FeMnAlSiC TRIP composition has been investigated. Two regular solution models have been derived to describe the two stage martensitic transformation (γ→ε→α') which has been observed via athermal and strain induced nucleation methods. Athermal transformation has been shown to produce a Shoji-Nishiyama orientation relationship between γ-austenite and ε-martensite while a Kurdjumov-Sachs orientation relationship has been observed for α-martensite nucleated from γ-austenite. Six crystallographic variants of α-martensite consisting of three twin-related variant pairs have been characterized in ε- bands. A planar parallelism of $\{0001\}\varepsilon \parallel \{110\}\alpha'$ and a directional relation of $<1\bar{1}1>\alpha'$ lying within 1° of $<\bar{1}2\bar{1}0>\varepsilon$ existed for these variants. The role of available nucleating defects of critical size, n^*, has been linked to the SFE necessary to observe the athermal γ→ε transformation and it is thus proposed that the amount of ε-martensite in the observed quenched microstructures is a function of material processing history as well as thermodynamic driving force. The developed regular solution models have been used as a predictive tool to determine optimized alloy compositions that produce ideal two-stage TRIP behavior. The influence of Mn, Si and Al on SFE and the γ→ε transformation as determined by the thermodynamic model has been shown to be in excellent agreement with ab-initio calculations. Aluminum was found to have the most significant influence on γ→ε driving force. Compositions with Al contents near 0.5 wt% have increased ε-martensite stability and are likely to lack sufficient amounts of retained austenite to produce Stage I TRIP (γ→ε). Compositions with Al contents near 1.5 wt% adequately

balance ε- and α-martensite start temperatures such that some retained austenite is expected upon quenching to room temperature while maintaining adequate transformation driving forces to ensure full two-stage TRIP behavior and avoid premature fracture. It has further been shown that two-stage TRIP behavior is probable in a Fe-12Mn-2.5Si-1.3Al-0.15C-0.017N composition where the lowering of Mn content may serve to increase alloy manufacturability via conventional continuous steelmaking operations.

BIBLIOGRAPHY

[1] J. Fekete and J. Hall: NIST Internal Report 6668, National Institute of Standards and Technology, Washington, DC, May 2012.

[2] D.K. Matlock and J.G. Speer: Proceedings of the 3rd Int. Conf. on Structural Steels, ed. By H.C. Lee, *The Korean Institute of Metals and Materials,* Seoul, Korea, 2006, pp 774-781.

[3] R.H. Wagoner: *Report on NSF-DOE-*AS*/P AHSS Workshop*, October 2006, Arlington, VA, pg. 21.

[4] E. Girault, A. Martens, P. Jacques, Y. Houbaert, B. Verlinden, J. Van Humbeeck: *Scripta Mater.*, 2001, vol. 44, pp. 885-92.

[5] V.F. Zackay, E.R. Parker, D. Fahr, R. Bush: *Trans ASM*, 1967, vol. 60, pp. 252-59.

[6] M.C. McGrath, D.C. Van Aken, N.I. Medvedeva, and J.E. Medvedeva: *Metall. Mater. Trans. A*, 2013, vol. 44A, pp. 4634-43.

[7] D.C. Van Aken, S.T. Pisarik, and M.C. McGrath: *Proc. Intl. Symp. Develop. AHSS*, 2013, Vail, Colorado, pp. 119-129.

[8] L. Bracke, L. Kestens, and J. Penning: *Scripta Mater.*, 2007, vol. 57, pp. 385–88.

[9] K. Spencer, J.D. Embury, K.T. Conlon, M. Veron, and Y. Brechet: *Mater. Sci. Eng. A*, 2004, vols. 387–389, pp. 873–81.

[10] S. Allain, J.P. Chateau, O. Bouaziz, S. Migot, N. Guelton: *Mater. Sci. Eng. A*, 2004, vols. 387-389, pp.158-62.

[11] O. Bouaziz and N. Guelton: *Mater. Sci. Eng. A*, 2001, vols. 319-321, pp. 246-49.

[12] M. Koyama, T. Sawaguchi, T. Lee, C.S. Lee, and K. Tsuzaki: *Mater. Sci. Eng. A*, 2011, vol. 528, pp. 7310-16.

[13] J.A. Venebles, R.J. de Angelis, and J.B. Cohen: *Metall. Soc. AIME*, 1963, vol. 25, pp. 77-116.

[14] S. Kibey, J. Liu, M. Curtis, D. Johnson, and H. Sehitoglu: *Acta Mater.*, 2006, vol. 54, pp. 2991-3001.

[15] G. Olson and M. Cohen: *Metall. Mater. Trans. A*, 1976, vol. 7, pp. 1897-1904.

[16] W.S. Yang and C.M Wan: *J. Mater. Sci.*, 1990, vol. 25, pp. 1821-23.

[17] P.J. Ferreira and P. Mullner: *Acta Mater.*, 1998, vol. 46, pp. 4479-84.

[18] N. I. Medvedeva, M. S. Park, D. C. Van Aken, and J. E. Medvedeva: *J. Alloys Compd.*, 2014, vol. 582, pp. 475-82.

[19] K.R. Limmer, D.C. Van Aken, and J.E. Medvedeva: *Proc. of AISTech 2014*, 2014, pp.1599-1605.

[20] H. Gholizadeh, C. Draxl, and P. Puschnig: *Acta Mater.*, 2013, vol. 61, pp. 341-49.

[21] J.A. Venables: *Phil. Mag.*, 1962, vol.7, pp. 35-44.

[22] A. Weidner, A. Glage, and H. Bierman: *Procedia Eng.*, 2010, vol. 2, pp. 1961-71.

[23] C.X. Huang, G. Yang, Y.L Gao, S.D. Wu, and S.X. Li: *J. Mater. Res.*, 2007, vol. 22 (3), pp. 724-729.

[24] J. Talonen and H. Hänninen: *Acta Mater.*, 2007, vol. 55, pp. 6108-18.

[25] J.F. Breedis and L. Kaufman: *Metall. Trans.*, 1971, vol. 2, pp. 2359-71.

[26] P.M. Kelly: *Acta Metall.*, 1965, vol. 13, pp. 635-46.

[27] D.L Manganon and G. Thomas: *Metall. Trans.*, 1970, vol. 1, pp. 1577-86.

[28] R. Lagneborg: *Acta Metall.*, 1964, vol. 12, pp. 823-43.

[29] G.B. Olson and M. Cohen: *J. Less-Common Met.*, 1972, vol. 28, pp. 107-18.

[30] S.T. Pisarik, D.C. Van Aken, K. Limmer, and J. Medvedeva: *Proc. of AISTech 2014*, 2014, pp. 3013-23.

[31] E.Yang, H. Zurob, and J. McDermid: *Proc. of MS&T'10*, 2010, pp. 1914-25.

[33] M. Koyama, T. Sawaguchi, and K. Tsuzaki: *Metall. Mater. Trans. A*, 2012, vol. 43, pp. 4063-74.

[34] B. Cina: *Acta Metall.*, 1958, vol. 6, pp. 748-62.

[35] I.V. Kireeva and Y.I Chumlyakov: *Phys. Met. Metallogr.*, 2006, vol. 101, pp. 186-203.

[36] H. Fujita and S. Ueda: *Acta Metall.*, 1972, vol. 20, pp. 759-67.

[37] G. Frommeyer, U. Brux, and P. Neumann: *ISIJ Int.*, 2003, vol. 3, pp. 438-46.

[38] A. Holden, J.D. Bolton, and E.R. Perry: *J. Iron Steel Inst.*, 1971, vol. 209, pp. 721-28.

[39] G. Frommeyer, U. Brux, and P. Neumann: *ISIJ Int.*, 2003, vol. 3, pp. 438-46.

[40] D.P. Koistinen and R.E. Marburger: *Acta Metall.*, 1959, vol. 7, pp. 59-60.

VITA

Scott Thomas Pisarik was born in St. Charles, MO. He received his B.S. in Metallurgical Engineering from Missouri University of Science and Technology in December 2012 having attended since August 2008. He remained at Missouri University of Science and Technology to pursue an M.S. in Metallurgical Engineering under Dr. David C. Van Aken from January 2013 until June 2014. He received his M.S. degree in August 2014.